

ARROWHEAD PATCH SLOT ANTENNA
FOR 5G APPLICATIONS

by
Yuhao Feng

Copyright by Yuhao Feng, 2020
All Rights Reserved

A thesis submitted to the Faculty and the Board of Trustees of the Colorado School of Mines in partial fulfillment of the requirements for the degree of Master of Science (Electrical Engineering).

Golden Colorado

Date _____

Signed: _____
Yuhao Feng

Signed: _____
Dr. Atef Z. Elsherbeni
Thesis Advisor

Golden, Colorado

Date _____

Signed: _____
Department of Engineering

ABSTRACT

With the rapid development of 5th generation mobile network (5G), the need to integrate multiple frequency bands and multiple wireless standards into 5G systems is growing. The antenna is an essential part of the system to ensure communication quality. Therefore, research on antennas and arrays suitable for the 5G frequency bands is of great significance for future wireless communication systems.

This thesis reviews recent antenna designs related to 5G systems, especially those based on coplanar waveguide feeding method. Then antenna based on coplanar waveguide feed structure is designed and optimized for better input impedance match and radiation performance. Measurements of the fabricated prototype confirmed the targeted operating frequencies. Furthermore, antenna array configurations are designed and optimized for 5G base stations or terminals. The scanning feature of the antenna array configurations (5 and 15 antenna elements) are investigated for operation in two segments of the licensed lower 5G frequency band (3.55-3.7GHz and 3.7-4.2GHz). Finally, a cavity is further suggested to be added to the bottom of the antenna element to focus the radiated field mainly in one half space and to be used in the array configurations.

Keywords: 5G antenna, coplanar waveguide, wide-band, multi-band, antenna arrays

TABLE OF CONTENTS

ABSTRACT	iii
LIST OF FIGURES	vi
LIST OF TABLES	viii
LIST OF SYMBOLS	ix
LIST OF ABBREVIATIONS.....	xi
ACKNOWLEDGMENTS	xii
DEDICATION	xiv
CHAPTER 1 INTRODUCTION	1
1.1 Research background	1
1.2 Research Status	2
1.2.1 Coplanar waveguide (CPW) antennas.....	2
1.2.2 Multi-frequency ultra-wideband (UWB) antennas.....	8
1.3 Thesis Contributions	8
CHAPTER 2 BASIC THEORY	10
2.1 Introduction	10
2.2 Electromagnetic Radiation	10
2.3 Microstrip Slot Antenna	10
2.3.1 Main electrical parameters of a microstrip antenna	11
2.4 Coplanar Waveguide Basic Principles.....	14
2.5 Chapter Summary	15

CHAPTER 3 MULTI-BAND ARROW PATCH-SLOT ANTENNA.....	16
3.1 Introduction.....	16
3.2 Design of Multi-band Arrow Patch-Slot Antenna Based on Coplanar Waveguide	16
3.2.1 HFSS results validation	17
3.2.2 Antenna design parameter	21
3.2.3 Validation of simulations and measurement results	22
3.3 Chapter Summary	25
CHAPTER 4 DESIGN OF ANTENNA ARRAY	31
4.1 Introduction.....	31
4.2 Design of Antenna Array Based on Arrow Patch-slot Antenna Element.....	32
4.2.1 Theoretical basis of antenna array	33
4.2.2 Basic structure configuration and parameter analysis of antenna array	34
4.2.3 Analysis of simulation results of antenna array	34
4.3 Chapter Summary	41
CHAPTER 5 CONCLUSIONS AND OUTLOOK	44
5.1 Summary	42
5.2 Future Work	43
REFERENCES CITED	45

LIST OF FIGURES

Figure 1.1	Antenna geometry from reference [21]	4
Figure 1.2	Measured and simulated S_{11} of the configuration from reference [21]	4
Figure 1.3	Antenna first resonant mode at 4 GHz: (a) Distribution of electric fields, (b) E -plane (yz -plane) patterns, and (c) H -plane (xz -plane) patterns.....	5
Figure 1.4	Antenna geometry from reference	6
Figure 1.5	Measured and simulated S_{11} for the antenna in reference	6
Figure 1.6	Simulated radiation patterns at different frequencies. (a) xz -plane (H -plane). (b) yz -plane (E -plane) of the antenna in reference.....	7
Figure 2.1	Block diagram for computing radiated fields by electric and magnetic current sources.	11
Figure 2.2	Microstrip antenna	12
Figure 3.1	The butterfly patch single element	17
Figure 3.2	The rectangle patch single element.....	18
Figure 3.3	The ellipse patch single element.....	18
Figure 3.4	Side structure of the CPW feed.	19
Figure 3.5	The current distribution and S_{11} of the arrow patch single element antenna	19
Figure 3.6	The arrow patch single element radiation pattern	20
Figure 3.7	S_{11} of different shapes of the antenna element.....	20
Figure 3.8	The single element of arrowhead antenna configuration.....	21
Figure 3.9	The sampled voltage vs. time at the antenna input port	22
Figure 3.10	Simulated and measured S_{11} at the low frequency band.....	23
Figure 3.11	Simulated and measured S_{11} at the high frequency band.....	23

Figure 3.12	Antenna measurement in chamber	24
Figure 3.13	Simulated far-field radiation pattern at 3.7 GHz	25
Figure 3.14	Simulated radiation pattern at 3.3 GHz	27
Figure 3.15	Simulated radiation pattern at 3.9 GHz	28
Figure 3.16	Simulated radiation pattern at 28 GHz	29
Figure 3.17	Simulated radiation pattern at 33 GHz	30
Figure 4.1	Configuration of a linear of 5-elements using CEMS	33
Figure 4.2	Configuration of a linear array of 15-elements using HFSS	33
Figure 4.3	S parameter at roots for the 1×5 linear arrays	35
Figure 4.4	5 elements liner array Gain Pattern at 3.7 GHz, uniform excitation with 0° main beam directions	36
Figure 4.5	5 elements liner array gain pattern at 3.7 GHz with uniform excitation and 30° main beam directions.....	36
Figure 4.6	5 elements liner array gain pattern at 3.7 GHz with uniform excitation and 45° main beam directions	37
Figure 4.7	S parameters at port 8 of a 15-element linear array using HFSS.....	38
Figure 4.8	15 elements liner array Gain Pattern at 3.7 GHz, uniform excitation with 0° main beam directions.....	40
Figure 4.9	15 elements liner array gain pattern at 3.7 GHz with uniform excitation and 45° main beam directions.	40
Figure 4.10	15 elements liner array gain pattern at 3.7 GHz with uniform excitation and 60° main beam directions.....	40
Figure 5.1	Cavity backed arrowhead slot antenna for unidirectional radiation pattern	43
Figure 5.2	S_{11} of cavity backed arrowhead slot antenna	43

LIST OF TABLES

Table 1.1	Microstrip line and CPW design and efficiency comparison	3
Table 3.1	Antenna structure data.....	21
Table 4.1	Excitation setting for (30° scanned beam)	35
Table 4.2	Excitation setting for (45° scanned beam)	36
Table 4.3	Excitation setting for 45° scanned beam.....	38
Table 4.4	Excitation setting for 60° scanned beam.....	39
Table 4.5	Broadside gain at 3.7 GHz	41

LIST OF SYMBOLS

Distance from the feed point to the corner	z
Energy storage at resonance	W_T
load impedance connected to feeder terminal.....	Z_L
Radiated power	P_{rad}
Equivalent dielectric constant	ϵ_e
Center working wavelength	λ_0
Cut-off frequency	f_r
Substrate thickness	h
Air permittivity	ϵ_0
Field strength in ϕ direction	E_ϕ
Substrate length.....	L
Substrate width.....	W
Band width	BW
Standing wave coefficient.....	S
Dielectric constant.....	ϵ_r
Conductance.....	G
Susceptance.....	B
Input admittance.....	Y_{in}
Characteristic admittance.....	Y_0
Directivity	D
Maximum directivity	D_{max}
Direction of maximum radiation.....	E_{max}

Radiation intensity	U
Maximum radiation intensity	U_{max}
Radiation intensity of isotropic source	U_0
Normalized field pattern	F

LIST OF ABBREVIATIONS

5 th generation wireless systems	5G
Coplanar waveguide.....	CPW
Voltage standing wave ratio	VSWR
Ultra-wideband	UWB

ACKNOWLEDGMENTS

During the past two years of my study as a Master student I have encountered many difficulties in my study and research, but at the same time I have enjoyed the process of obtaining results and solving problems. As I am about to enter the next stage of my life, I would like to express my sincere gratitude to my teachers, friends and relatives who have offered me enormous help and support over the last two years.

First, I would like to thank my supervisor Dr. Atef Z. Elsherbeni. In academic research and course guidance, he has guided me on how to carry out scientific research all the way through my study and given me numerous valuable suggestions. From joining the ARC research group to the completion of the final thesis, my supervisor Dr. Elsherbeni has provided a lot of support and help. At the same time, I also have learned a lot from him. His serious attitude to research and problems is something I admire and need to aspire towards. Special thanks and tribute to Dr. Elsherbeni.

Thanks to Dr. Mohammed Hadi for his insights on this research. During the weekly group meeting, Dr. Hadi has put forward questions, opinions, and solutions to our research, which facilitated me to think critically. Thanks to Professor Fan Yang of Tsinghua University for assisting me with antenna fabrication and measurement. I also would like to thank other members of the ARC lab, including Joseph Diener, Alec Weiss, Joshua Kast, Abdullah Algarni, Yiming Chen, Robert Jones, Madison Le, Tony D'Esposito, Allison Tanner, Rachel Lumnitzer, Andy, Velasco and Kyle Patel. Through communication with them, I have learned a lot of theoretical knowledge and research skills during the past two. Thanks again to Dr. Atef Z. Elsherbeni, Dr. Mohammed Hadi and Dr. Peter Aaen for taking the time to review this thesis and giving me guidance and suggestions.

At the same time, I also would like to thank my family and friends for their support and care all these years to keep me moving forward.

Thanks also to my childhood idol Kobe Bryant. Although he unfortunately died, his “Mamba Mentality” has always encouraged me and taught me never to give up and retreat.

The research in this thesis was partially supported by the gift funds from Futurewei Technology Inc., New Jersey Research Center, Bridgewater, NJ, USA.

This thesis is dedicated to my wonderful time spent studying in the United States.

CHAPTER 1

INTRODUCTION

1.1 Research background

Antennas are used in wireless communication systems to transmit and receive electromagnetic waves. Their performance is an important factor in determining the system's efficiency. It is clear that countries and companies, who are developing 5G communication systems, are competing fiercely for the frequency spectrum [1]. Increasing the utilization of the spectrum poses challenges to the requirements imposed on the antenna designers.

The density of circuit components of recent and future wireless devices and wireless terminal products increases while the device size is getting smaller and at the same time is required to support a wide band of frequency. As a result, the antenna in wireless electronic devices must be carefully designed to conform with the smaller requirements [2–5] while continues to support the working bandwidth. The requirements of 5G, such as larger bandwidth and faster communications are constantly increasing. As a result, the number of required antennas in a system is constantly increasing, which will increase the volume, weight and cost of the related devices. In some applications it is further required that the antenna can support multiple working frequency bands. Due to the above reasons, and because the size of mobile wireless devices is getting smaller and smaller, the space left for the antenna is also smaller. Considering these factors, if multiple separate antennas are used to cover multiple operating frequency bands, the entire system will not only increase in size, but will also become complex in terms of the cross-coupling between the existing antennas. The resulting electromagnetic interference usually reduce the communication quality. Therefore, designing a single small antenna with the characteristics of multiple antennas has become a topic of important research [6–12]. The single antenna operating at multi or wide band frequencies ensure the miniaturization of wireless communication terminals or 5G base stations. The need of miniaturization and multi-mode antenna integration in electronic equipment has been a contentious research area as demonstrated in [13, 14].

For the design of a 5G antenna, it is evident that the use of a coplanar waveguide (CPW)

structure [15–19] as a feed for the antenna is conducive to connecting other passive and active circuit components. Such unique structure also facilitates antenna feeding, especially in an array configuration. There are several publications on coplanar waveguide structures acting as feed for antennas that provide good radiation characteristics such as bandwidth, gain and low sidelobe levels [20-22]. Few of these available CPW-antenna designs are investigated, among which are the butterfly-shaped antenna and the rectangular wide-slot antenna.

Future 5G communication systems face challenges such as cost and weight reduction, good electromagnetic compatibility, multi-functional integration and system miniaturization. Thus the intention of this thesis is to design a micro-strip patch antenna based on a coplanar waveguide (CPW) feed that can support the operation in the lower and higher frequency bands of a 5G system while using CPW feeding structure to simplify the addition of circuitry of the RF front end.

1.2 Research Status

1.2.1 Coplanar waveguide antennas

In recent years, with the increasing demand for wireless communication and the development of millimeter wave technology, broadband and dual-frequency wireless communication technologies have been widely used. The improvement of passive device performance and the emergence of new devices have promoted the continuous development of wireless communication technology. Coplanar waveguide (CPW) is a very important microwave transmission line analogues to the planar transmission structure that was first proposed in 1969 [23]. Microstrip lines show many deficiencies in many aspects, such as dispersion. On the other hand, coplanar waveguides have the advantages of low loss, and ease of serial and parallel connection with other circuits and devices. The following table compares the design and manufacturing performance of microstrip lines and coplanar waveguides:

Table 1.1: Microstrip line and CPW design efficiency comparison

	Property	Microstrip Line	CPW
Design Aspect	Dispersion	High	Low
	Loss	Low	High
	Coupling	High	Low
	Design flexibility	Low	High
Manufacturing	Circuit size	Large	Small
	Back modeling	Need	Not needed

In order to meet the system volume and size requirements of modern 5G communication equipment, the antenna is also required to be in low profile, miniaturized, and provides wideband frequency operation. The co-planer waveguide feed structure can effectively broaden the impedance bandwidth of the antenna. CPW has two feeding modes, one without a ground plane under the substrate and the other with full ground plane and is usually called GCPW. For the antennas investigated in this thesis a partial ground plane will be used.

The structure shown in Fig 1.1 presents a configuration of a rectangular slot patch antenna fed by a CPW [24]. The corresponding S_{11} versus frequency is shown in Fig 1.2, while the distribution of the electric field at 4 GHz and the radiation patterns in the E and H planes are shown in Fig 1.3. From the figure, we can see that the CPW feeding method can achieve better feeding bandwidth and good CP radiation patterns. Another antenna configuration of a circular patch/slot antenna structure is shown in Fig 1.4 [25]. The antenna uses a circular microstrip patch as the radiating unit. The S_{11} characteristic curve and radiation pattern of this antenna are shown in Figs. 1.5 and 1.6, respectively. We can see that the circular microstrip antenna using CPW as the feeding structure yields a wide impedance bandwidth and relatively consistent directivity pattern versus frequency.

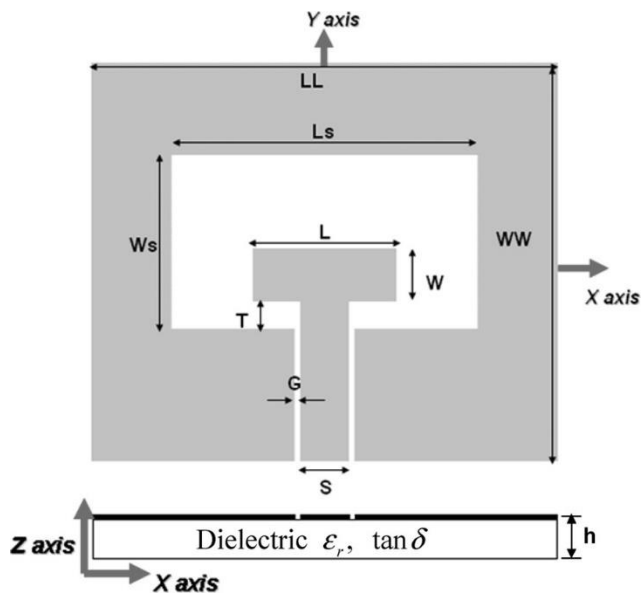


Figure 1.1: Antenna geometry from reference [24].

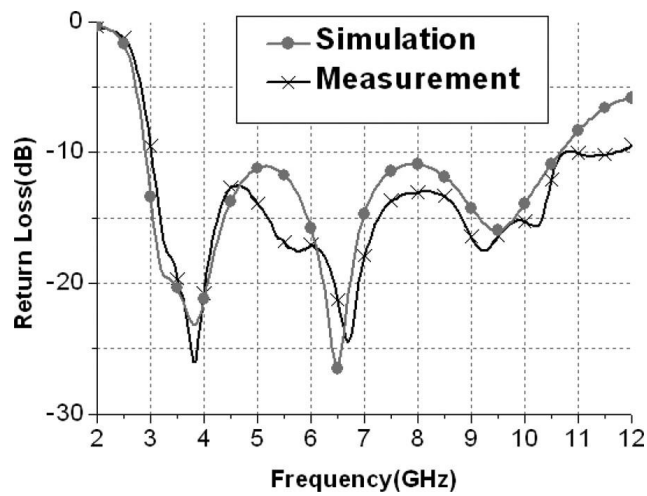
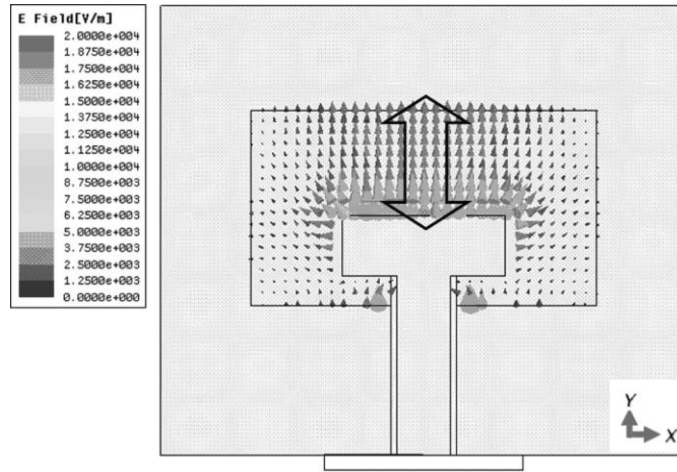
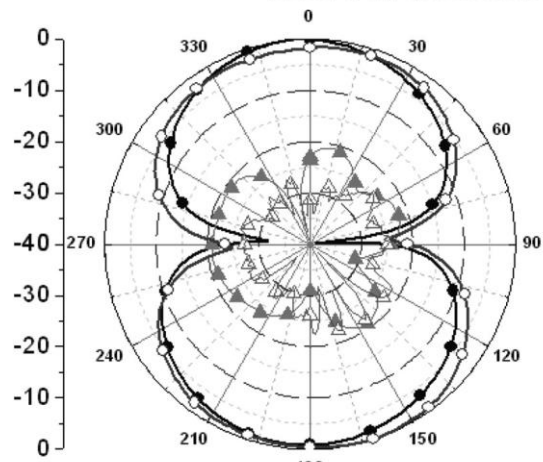


Figure 1.2: Measured and simulated S_{11} of the configuration from reference [24].



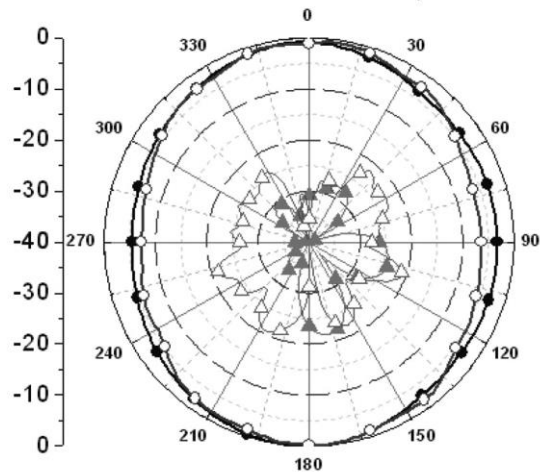
(a)

● Co Pol. ▲ Cross Pol. (Simulation)
 ○ Co Pol. △ Cross Pol. (Measurement)



(b)

● Co Pol. ▲ Cross Pol. (Simulation)
 ○ Co Pol. △ Cross Pol. (Measurement)



(c)

Figure 1.3: Antenna first resonant mode at 4 GHz: (a) Distribution of electric fields, (b) E -plane (yz -plane) patterns, and (c) H -plane (xz -plane) patterns [24].

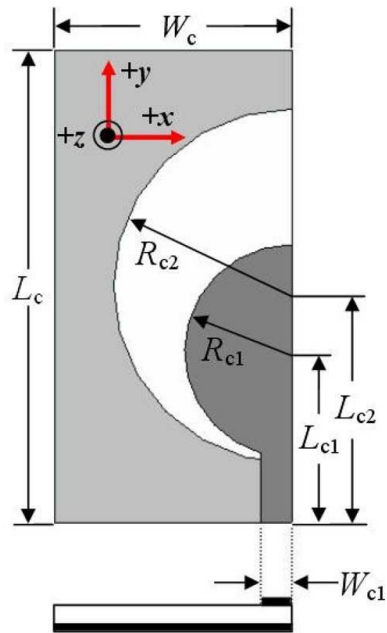


Figure 1.4: Antenna geometry from reference [25].

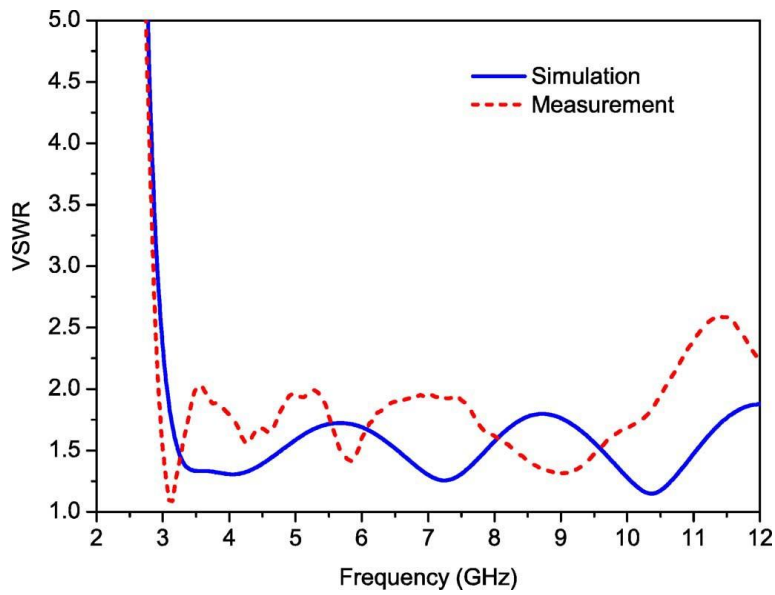
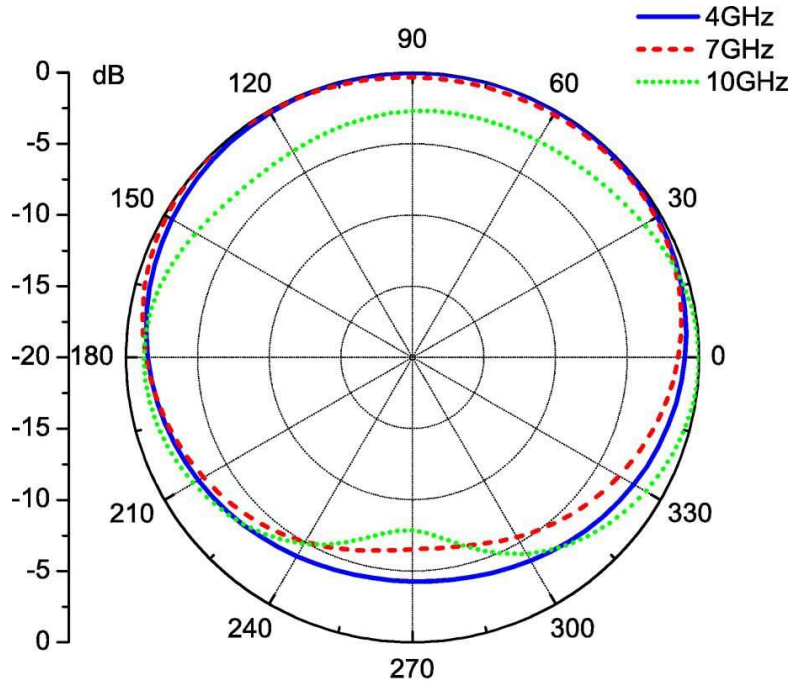
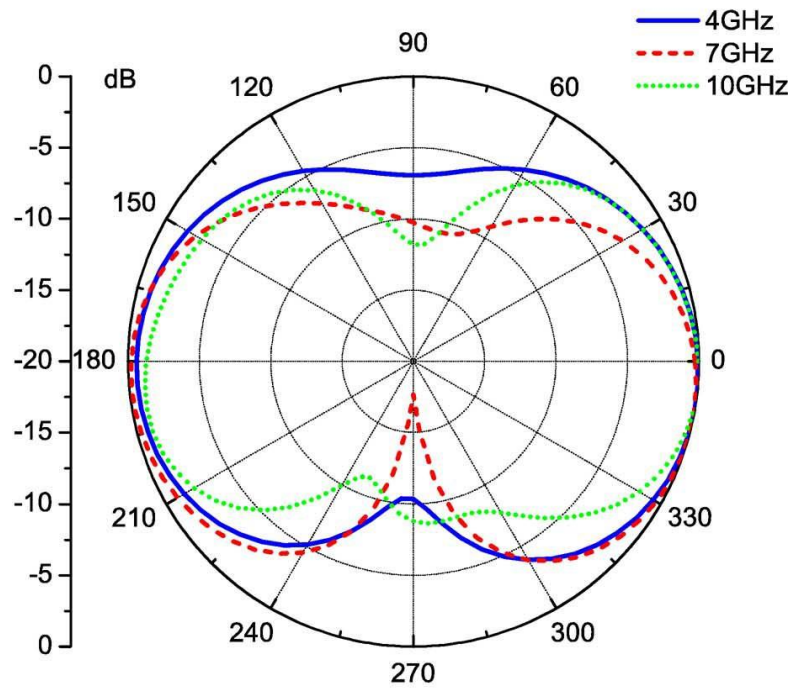


Figure 1.5: Measured and simulated S_{11} for the antenna in reference [25].



(a)



(b)

Figure 1.6: Simulated radiation patterns at different frequencies. (a) xz -plane (H -plane). (b) yz -plane (E -plane) of the antenna in reference [25].

1.2.2 Multi-frequency wideband antennas

In 1943, Oliver designed the first bi-conical antenna with wideband operating characteristics [26]. This antenna was used for the transmission and reception of radio telegraphs, but the structure of the bi-conical antenna was large. Later, Amrolah et.al. introduced the concept of fractal for the first time in the design of a log- periodic antenna, using a rectangular fractal structure as the periodic unit, thereby achieving miniaturization of the antenna and constant radiation gain over the operating band [27–29]. With the multiple periodic units being used, constant radiation gain over the band are achieved. However, since it is necessary to use a plurality of periodic units, it is difficult to reduce the size of the antenna. With the rise of mobile terminal equipment, research into the application of these antennas in wideband communications has gradually increased.

Nowadays, the research on wideband or multi-frequency antennas has been biased towards the use of flat printed monopoles, dipoles, slot antennas and other types of electrical small antennas [30–32]. This type of antenna is easier to implement as a compact structure and easy to integrate with peripheral circuits, and has the advantages of wide impedance bandwidth, good far-field radiation characteristics, and small dispersion characteristics; hence it is the focus of mainstream research of wideband antennas.

Since the lower and higher 5G frequency bands are separated by more than 10 octaves, it would be a good choice to design an antenna operating at the two frequency bands with reasonable bandwidth within each band.

1.3 Thesis Contributions

Based on the above background and development trends, this thesis mainly aims towards the design of antennas for two 5G frequency bands. By using a coplanar waveguide patch-slot structure and optimizing the design through simulation software, the problems of miniaturization and multi-frequency operation for 5G application is achieved.

Based on the research and background of 5G antennas, chapter 1 investigates the design of a broadband or a multi-frequency antenna with a coplanar waveguide feeding structure. The design of the antenna was geared towards miniaturization, broadband, and multiple operating modes.

The second chapter introduces the basic theoretical knowledge and the design of a single antenna related to the research in this thesis. It is divided into three parts. First, the basic theory of electromagnetic radiation is summarized. Then the parameters and concepts of the microstrip antenna are briefly analyzed. Finally, the design structure of the coplanar waveguide antenna is analyzed and explained. Compared with the microstrip feeding structure, the advantages and disadvantages of the coplanar waveguide structure are discussed.

In Chapter 3, a microstrip/slot patch antenna with CPW feed is designed for 5G low and high frequency bands. Through continuous analysis and simulation, the antenna can cover two of the lower frequency bands at 3.1 GHz, and 5.4 GHz. With an additional resonance at 28 GHz to cover the higher frequency band of the 5G standard in the United States. A prototype of this antenna was fabricated, and the measurement of the input impedance bandwidth and operating frequencies are conducted. It is found that the measured results are closely matched the simulation results at low frequencies, but some differences at high frequencies are observed which are due to the use of improper substrate material and connector type for the high frequency band.

In Chapter 4, two configurations of antenna arrays are designed based on the element antenna designed in Chapter 3. The simulation results are obtained for two different numbers of elements in two antenna array configurations for potential use in 5G base stations. Scanning capabilities of the two arrays are examined. The results encourage further investigations to improve the design of the single antenna element to better fit in a larger configuration of antenna arrays.

Finally, Chapter 5 summarizes the research conducted in this thesis and proposes possible research areas for future related work.

CHAPTER 2

BASIC THEORY

2.1 Introduction

The theory of electromagnetic radiation is the theoretical basis for analyzing antennas. This chapter first discusses the basic theory of electromagnetic radiation, briefly describes the method of obtaining the electromagnetic field distribution in free space and analyzes the indirect acquisition methods in detail. Theoretical analysis of the microstrip antenna was carried out to provide the equations and characteristics of the input impedance and the far field distribution.

2.2 Electromagnetic Radiation

Electromagnetic radiation at any point in space can be determined from the existing distribution of the electric and magnetic currents (\mathbf{J} and \mathbf{M}). The corresponding electric and magnetic fields (\mathbf{E} and \mathbf{H}) can be evaluated through direct integration with the kernel contains \mathbf{J} and \mathbf{M} . However, this direct process is complicated specially if one is looking for the far field's quantities only. An alternative procedure is composed of two steps as illustrated in Fig. 2.1. First, the auxiliary vector potential \mathbf{A} and \mathbf{F} are evaluated through simple integration, then the far field radiation component is evaluated using simple multiplication factor.

2.3 Microstrip Slot Antenna

The microstrip slot antenna advantage is that it can generate a bi-directional or uni-directional pattern with or without the use of a ground plane. In the design of the microstrip patch-slot antenna, a combination of a patch and a slot is used. For the ground plane configuration, a metal thin layer is attached on one side of a dielectric substrate as a ground plate, and on the other side, a metal sheet with a slot large enough to host a patch of a certain shape. The patch is then fed by a microstrip line, CPW, or a coaxial probe.

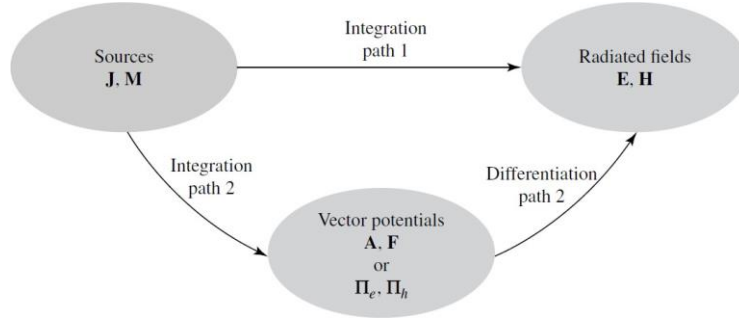


Figure 2.1: Block diagram for computing radiated fields by electric and magnetic current sources [33].

2.3.1 Main electrical parameters of a microstrip antenna

Input impedance or input admittance is a fundamental parameter, which needs to be accurately calculated when designing the antenna that achieves a good match between the antenna element and the feed. For a microstrip antenna, the input admittance can be calculated using Equation 2.1:

$$Y_{in}(z) = 2G \left[\cos^2(\beta z) + \frac{G^2 + B^2}{Y_0^2} \sin^2(\beta z) - \frac{B}{Y_0} \sin(2\beta z)^{-1} \right] \quad (2.1)$$

Where z is the distance from the feed point to the microstrip edge, and the propagation constant β is given as $B = \frac{k_0 \Delta l \epsilon_e}{Z_0}$

In practice, $\frac{G}{Y_0} \ll 1$ and $\frac{B}{Y_0} \ll 1$, this gives the formula 2.2:

$$Y_{in}(z) = \frac{2G}{\cos^2(\beta z)} \quad (2.2)$$

Y_{in} is input admittance, Y_0 is characteristic admittance, B is susceptance, G is conductance.

For co-axially fed microstrip antennas, the input impedance is given as

$$Z_{in} = Z_L + jX_L, \left(Z_L = \frac{1}{Y_L} \right) \quad (2.3)$$

Z_{in} is input impedance, Z_L is load impedance, X_L is inductance.

The radiation resistance can be determined according to the patch width W and working wavelength λ_0 as:

$$R_r = \frac{90\lambda_0^2}{W^2} \text{ for } W \ll \lambda_0$$

$$R_r = \frac{120\lambda_0}{W} \text{ for } W \ll \lambda_0 \quad (2.4)$$

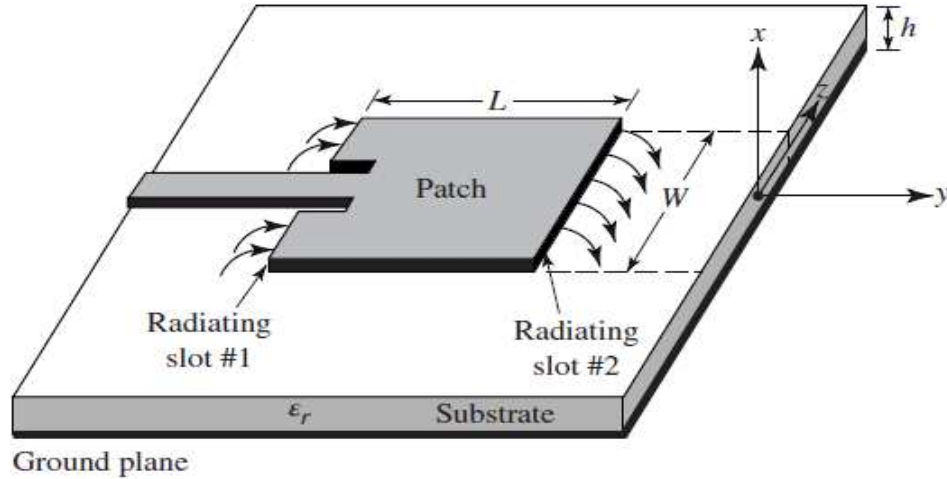
The quality factor related to radiation resistance is

$$Q_r = \frac{2\pi f_r W_T}{P_r} \quad (2.5)$$

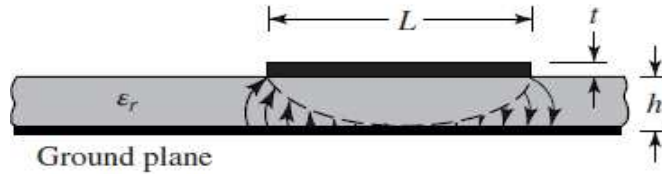
When using the formula $W_T = \frac{1}{4} \epsilon_0 \epsilon_r E_\phi^2 h L W$, the simplified form of the quality factor is:

$$Q_r = \frac{c \epsilon_e}{4 f_r h} \quad (2.6)$$

Where W and L are the dimensions of the microstrip patch, W_T is the energy storage at resonance, and P_r is the radiated power. ϵ_0 is air permittivity, ϵ_r is dielectric permittivity, E_ϕ is field strength in ϕ direction, ϵ_e is equivalent dielectric constant, h is substrate thickness and f_r is resonance frequency.



(a) Microstrip antenna



(b) Side view

Figure 2.2: Microstrip antenna [33].

The microstrip antenna bandwidth can be approximated in terms of the standing wave S and the quality factor as:

$$BW = \frac{S-1}{Q_r S} \quad (2.7)$$

One of the disadvantages of microstrip antennas is its bandwidth which is usually narrow. Therefore, many studies have proposed many methods to increase the bandwidth, for example, using parasitic patches of similar size, or a thicker substrate or a substrate with a lower dielectric constant ϵ_r , and the use of different shapes of patches or feeding structure.

The directivity D is the ratio of the power density of the antenna at a point in the far zone in the maximum radiation direction to the power density of the non-directional antenna with the same radiated power at the same point and can be expressed as:

$$D = \frac{|E_{max}|^2}{|E_0|^2} \Big|_{P_r=P_{r0}} \quad (2.8)$$

Where E_{max} is the direction of maximum radiation.

Directivity of an antenna defined as “the ratio of the radiation intensity in a given direction from the antenna to the radiation intensity averaged over all directions as if it is an isotropic source [33]

$$D(\theta, \phi) = \frac{U}{U_0} = \frac{4\pi U}{P_{rad}} \quad (2.9)$$

If the direction is not specified, it implies the direction of maximum radiation, maximum directivity is then defined as:

$$D_{max} = \frac{U_{max}}{U_0} = \frac{4\pi U_{max}}{P_{rad}} \quad (2.10)$$

Where D is directivity, D_{max} is maximum directivity, U is radiation intensity (W/unit solid angle), U_{max} is maximum radiation intensity (W/unit solid angle), U_0 is radiation intensity of isotropic source (W/unit solid angle), P_{rad} is total radiated power (W).

The normalized radiation pattern of the antenna can be written in spherical coordinates as a function:

$$F(\theta, \phi) \quad (2.11)$$

With this normalized radiation pattern, the directivity can be computed as:

$$D(\theta, \phi) = \frac{4\pi}{\int_0^{2\pi} \int_0^\pi F^2(\theta, \phi) \sin\theta d\theta d\phi} \quad (2.12)$$

where θ and ϕ are the spherical coordinates.

2.4 Coplanar Waveguide Basic Principles

A traditional coplanar waveguide is a printed conductor strip on a dielectric substrate. A coplanar waveguide contains a pair of conductor planes on both sides of the printed conductor strip (the conductor plane is symmetrical to the conductor strip and is on the same plane as the conductor strip, so it is called "coplanar"), which are named as return conductors. This pair of return conductors are separated from the center conductor strip with a very small gap. The return conductors usually extend to a large distance in a direction away from the center conductor and in some approximate analysis are considered semi-infinite planes.

A coplanar waveguide with a ground plane is also called grounded coplanar waveguide (GCPW). Compared to a microstrip line feed, a grounded coplanar waveguide has a ground plane not only on the bottom of the dielectric substrate but also on both sides of the signal transmission line on the top of the dielectric substrate. The GCPW achieves constant electrical performance by surrounding the signal line with a ground plane. The transmission modes of microstrip feed lines and grounded coplanar waveguide circuits are both quasi-transverse electromagnetic modes. Because of the enhanced ground structure of the GCPW circuit, its machining is also more complicated to a certain extent. Compared with microstrip lines, GCPW circuits have low dispersion characteristics. When the frequency rises to the millimeter wave band, GCPW circuits also have lower radiation losses than microstrip line circuits. Due to the enhanced ground structure, the GCPW circuit has a wider effective bandwidth and a larger impedance range than a microstrip line circuit. However, the microstrip line circuit structure is relatively simpler to fabricate. In a microstrip line circuit, the electromagnetic field is mostly distributed between the top signal plane and the bottom ground plane, and the signal conductor edge has a strong field distribution. In GCPW circuits, the electromagnetic field is mainly distributed between the ground plane-signal line-ground plane (GSG) areas on the coplanar circuit layer. The field distribution between the top signal plane and the bottom ground plane of the GCPW circuit is weaker than that of a microstrip line circuit. The conductor loss of GCPW circuit is higher than that of the microstrip line, but its adjacent ground plane structure has lower radiation loss and is more conducive to suppressing

parasitic mode. Even if there are some inconsistencies in the circuit processing technology, the microstrip line circuit can still provide more stable and consistent circuit performance. GCPW circuits have lower losses when operating in high frequency bands, but GCPW circuit performance is more susceptible to processing technology effects. Most of the electromagnetic field energy of the GCPW circuit is transmitted through air with a dielectric constant of 1 rather than through a conductive metal or dielectric material with a high dielectric constant, which results in a lower effective dielectric constant of the GCPW circuit. The wide conductor used helps reduce conductor losses. In addition, the thick copper structure of the GCPW circuit makes the circuit have higher conductor walls, which will also increase the electromagnetic energy transmitted in the air space around the copper conductor and reduce the effective dielectric constant and the circuit loss.

In general, microstrip circuits in the microwave band have lower losses than GCPW circuits, especially when there are processing differences. However, when the frequency is gradually increased even to the millimeter wave band, the GCPW circuit will have both lower dispersion as well as radiation loss and a wider bandwidth relative to the microstrip line circuit.

2.5 Chapter Summary

This chapter first introduces the basic theory of electromagnetic radiation and microstrip antenna design and its main electrical parameters. Then, the far radiation field relation with the electric and magnetic source are shown. Then, the coplanar waveguide structure is described, and its electrical characteristics are highlighted. The advantages of the coplanar waveguide relative to microstrip lines finally lay the foundation of the design of the antenna in this thesis.

CHAPTER 3

MULTI-BAND ARROW PATCH-SLOT ANTENNA

3.1 Introduction

In 2013, the Federal Communications Commission (FCC) proposed the concept of 5G [1], and the FCC finally determined the range of the 5G frequency band. Divided into low frequency band, middle frequency band and high frequency band, and open this technology for commercial use. Because of its advantages, such as its high transmission rate and low power spectral density, the application of multi-frequency broadband technology has attracted widespread attention and has achieved significant development and progress in recent years. A large amount of research focuses on how to achieve miniaturization, broadbandization, and stable far-field characteristics of antennas for 5G applications. This chapter designs and studies the two frequency segments in the low-band, that is 3.55-3.7 GHz and 3.7-4.2 GHz, and the high-band 27.5-28.35 GHz of 5G. The use of coplanar waveguides and the shape and type of radiating antenna element facilitate the design for multi-frequency bands.

In this chapter, a coplanar waveguide wide-slot antenna is first designed. The coplanar waveguide excites planar elliptical, rectangular and butterfly shaped monopole antennas. The arrow-shaped patch antenna is stimulated for performance comparison. By adjusting the size of the arrow-patch and the size of the slit, the antenna's working frequency band covers the 5G low and high frequency bands proposed by the FCC. The antenna was fabricated and measured to determine its characteristics at 3.7GHz and 28GHz.

3.2 Design of Multi-band Arrow Patch-Slot Antenna Based on Coplanar Waveguide

This section presents the proposed design of an antenna element through simulation results supporting a multi-frequency microstrip patch antenna based on a coplanar waveguide. The designed antenna is matched for operation in the 5G low and high bands.

3.2.1 HFSS simulation results

In the initial design, different shapes of patch antennas were investigated. When the patch antenna was in the shape of a butterfly, the resonance obtained was not supporting sufficient bandwidth, see Fig. 3.1. The patch is then changed to a rectangular shape resulting in an operating frequency from 4.9 GHz to 5.9GHz. This antenna structure and simulation results are shown in Figure 3.2. When the patch the antenna is changed to an oval shape, as shown in Figure 3.3, one can see that the working frequency band is from 5.18GHz to 4GHz. The performance of the antenna is improved, the resonance point depth is increased, and the bandwidth is widened, but at a frequency higher than the designated frequency segments in the low band. Therefore, efforts to modify the resonance point (to move the resonance point to the left within the required operating frequency band) and increase the bandwidth while reduce the patch size. It should be mentioned that the GCPW feed structure of the antenna was also optimized and a short metal on the side of the feeder is added, as shown in Figure 3-4 to improve the antenna's bandwidth at low frequencies. Optimization is performed on the arrow-shaped patch to obtain a wide bandwidth of 2.86-5.97 GHz, as shown in Figure 3.5. The current distribution for this antenna configuration is also shown and the corresponding 3D radiation pattern is shown in Fig. 3.6 at 3.7 GHz. It can be seen from Fig. 3.7 that the antenna's operating bandwidth is different due to the different shapes of the patch area.

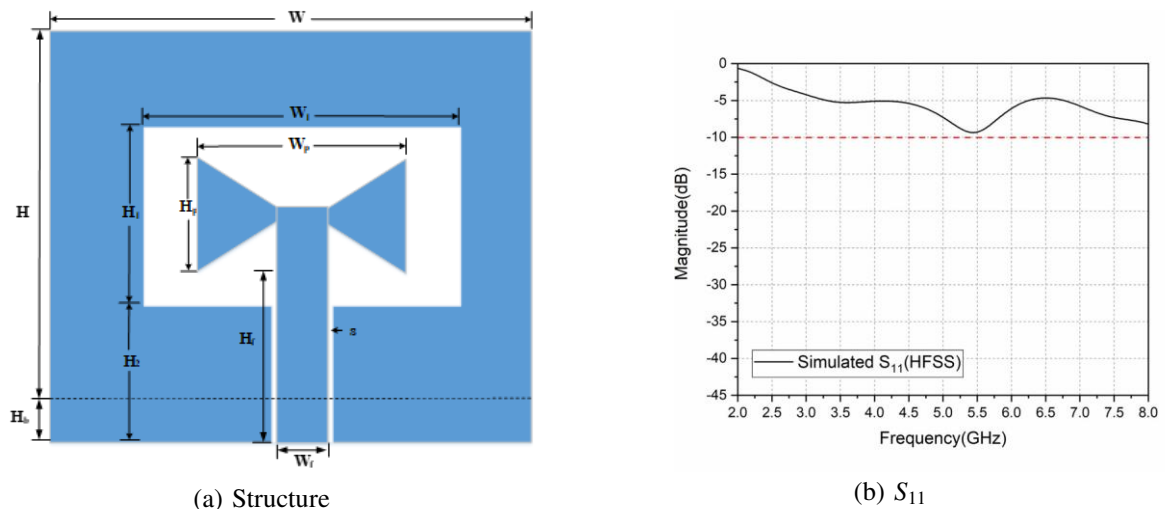
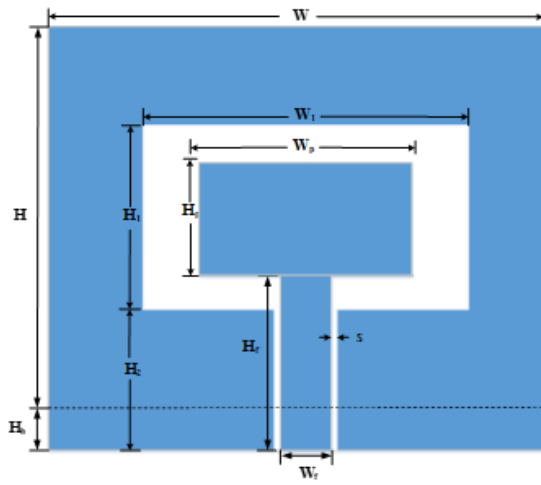
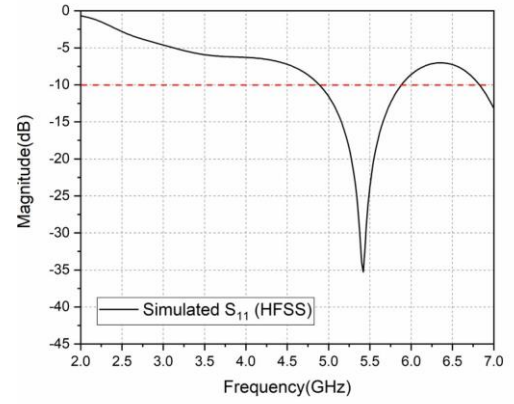


Figure 3.1: The butterfly patch single element antenna.

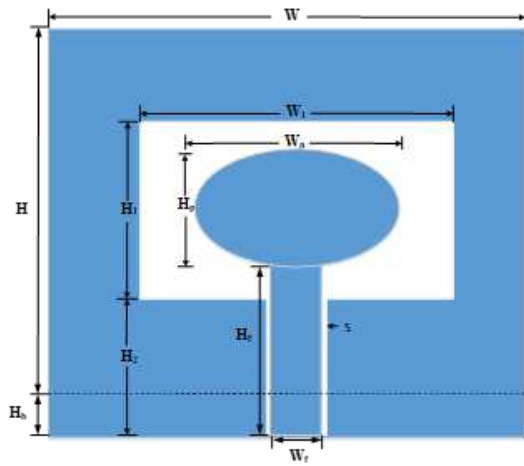


(a) Structure

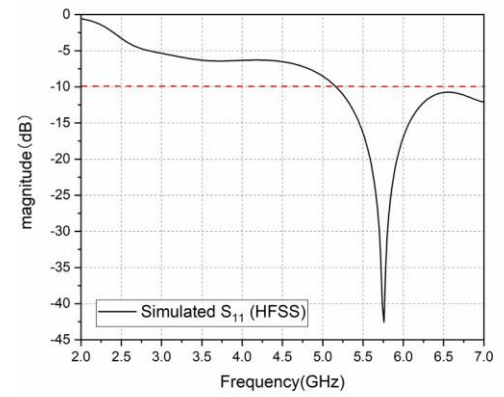


(b) S_{11}

Figure 3.2: The rectangle patch single element antenna.



(a) Structure



(b) S_{11}

Figure 3.3: The ellipse patch single element antenna.

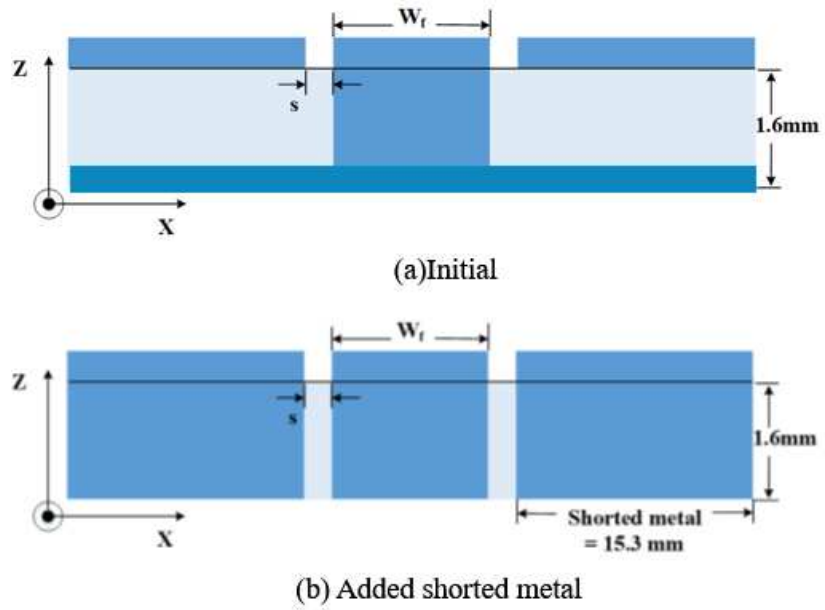


Figure 3.4: Side structure of the CPW feed.

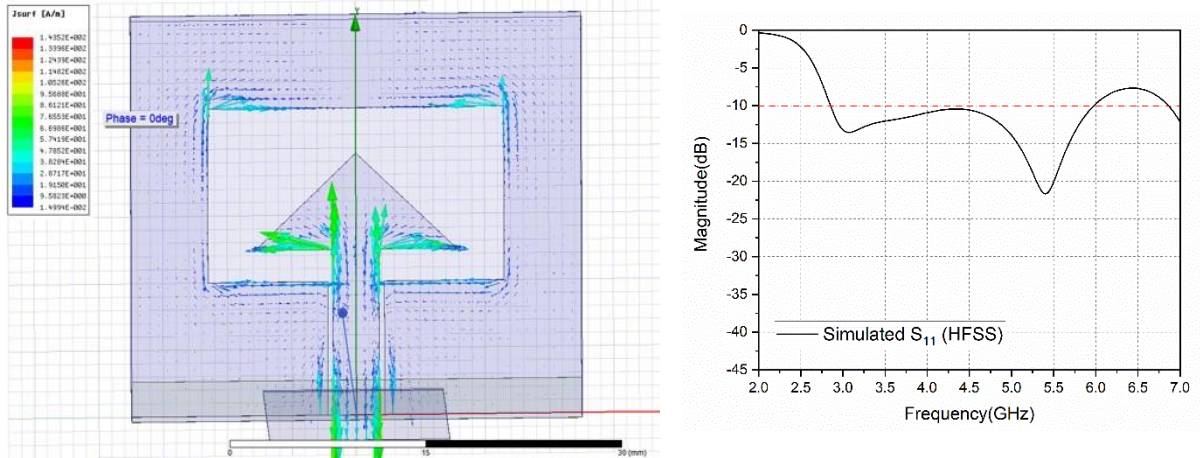


Figure 3.5: The current distribution and S_{11} of the arrow patch single element antenna.

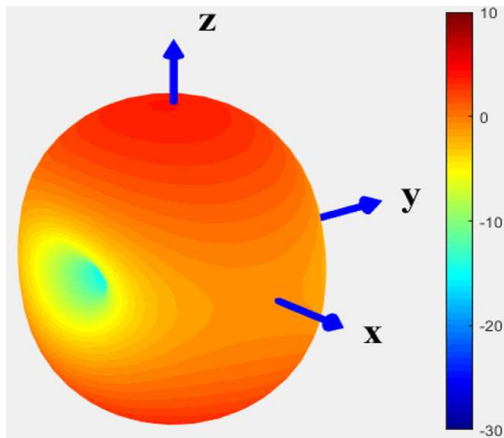


Figure 3.6: The arrow patch single element radiation pattern.

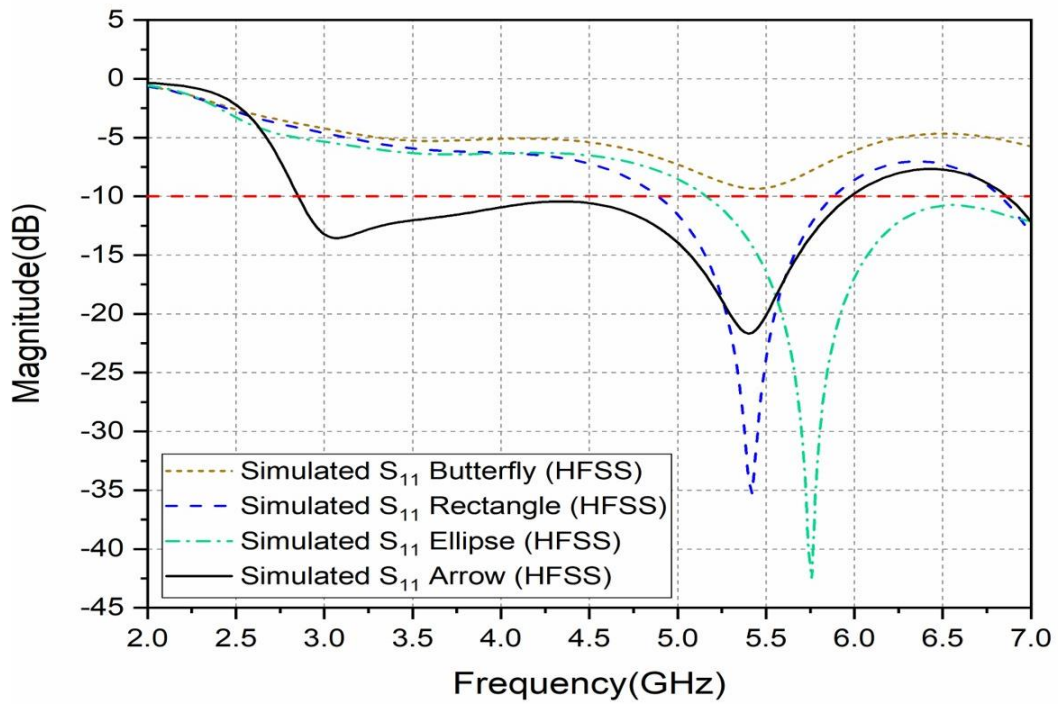


Figure 3.7: S_{11} of different shapes of the antenna element.

3.2.2 Antenna design parameters

The top view of the proposed antenna element is shown in Fig. 3.8 along with the fabricated prototype, with substrate thickness of 1.6 mm, relative permittivity of 4.4, and loss tangent of 0.02. The footprint size of this antenna is $35(W) \times 30(H)$ mm², which are $0.43\lambda \times 0.37\lambda$ at 3.7 GHz. The dash line in Fig. 3.8(a) represents a partial metal ground plane at the bottom side of the substrate with dimensions of $35(W) \times 3(H)$ mm². The other dimensions of the antenna element in millimeters are listed in the table 3.1:

Table 3.1: Antenna structure data

$W = 35$	$H = 30$	$W_1 = 23$	$H_1 = 13$	$H_2 = 10$	$W_p = 15.6$
$H_p = 7.2$	$W_f = 3.6$	$H_f = 12.4$	$s = 0.4$	$H_b = 3$	

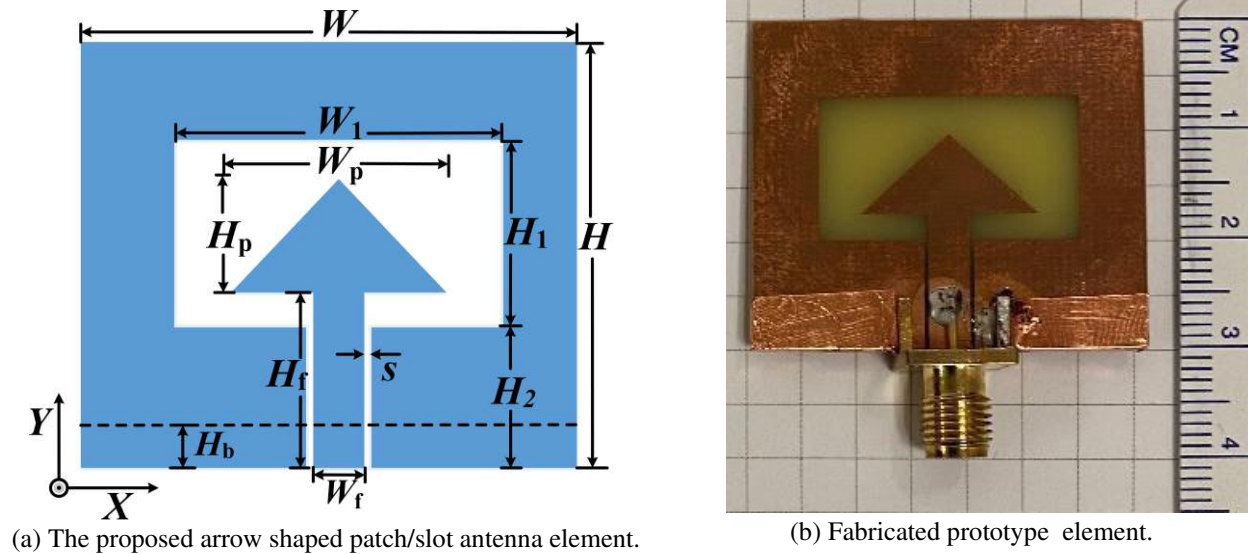


Figure 3.8: The single element of arrowhead antenna configuration.

3.2.3 Validation of simulations and measurement results

In order to validate the setup and the resulting numerical simulations from HFSS, another full wave simulation software CEMS [34] which is based on the time-domain finite difference method (FDTD) method [35] but running on GPU is used. . The setup in CEMS was as follows: cell size $0.1 \times 0.1 \times 0.1 \text{ mm}$, the cmpl thickness is 10 cells, and the excitation waveform supporting frequencies up to 50 GHz with a frequency step to 0.02 GHz. To validate the frequency domain results, time domain results were first examined for complete waveform response. As an example, the time domain sampled voltage signal at the antenna input port is shown in Fig. 3.9. The figure revealed that sufficient time steps are used, and that the computational domain absorbing boundary is effective in suppressing any artificial.

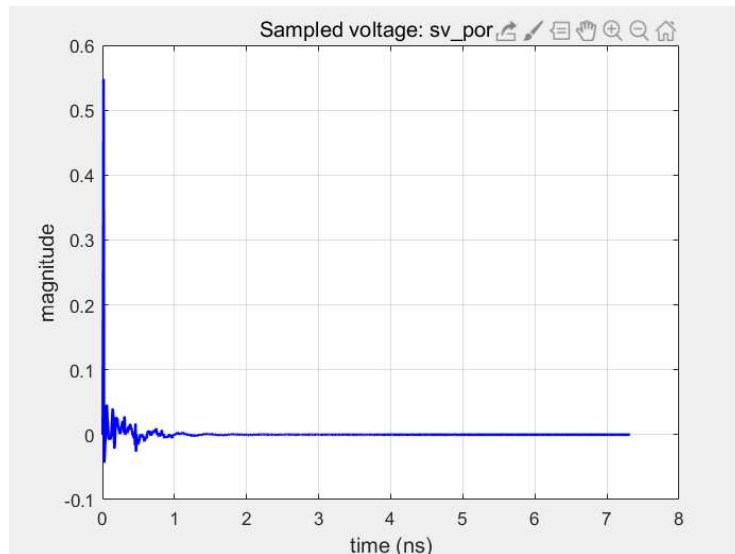


Figure 3.9: The sampled voltage vs. time at the antenna input port.

In Fig. 3.10 the corresponding S_{11} at the input port of the antenna is presented based on two different simulations (HFSS and CEMS) and compared with the measured results conducted at the antennas and RFID computational (ARC) lab in the EE department at Mines. Good match is clearly shown from 2.9 GHz to 5.9 GHz which contains the two licensed frequency segments (3.55-3.7 GHz and 3.7-4.2 GHz.) of the low band. In house measurement facilities for the higher frequency band are not available and hence the antenna measurement of the S_{11} in the high frequency range

as shown in Fig. 3.11 is performed in the microwave chamber of Tsinghua University in China (shown in Fig. 3.12).

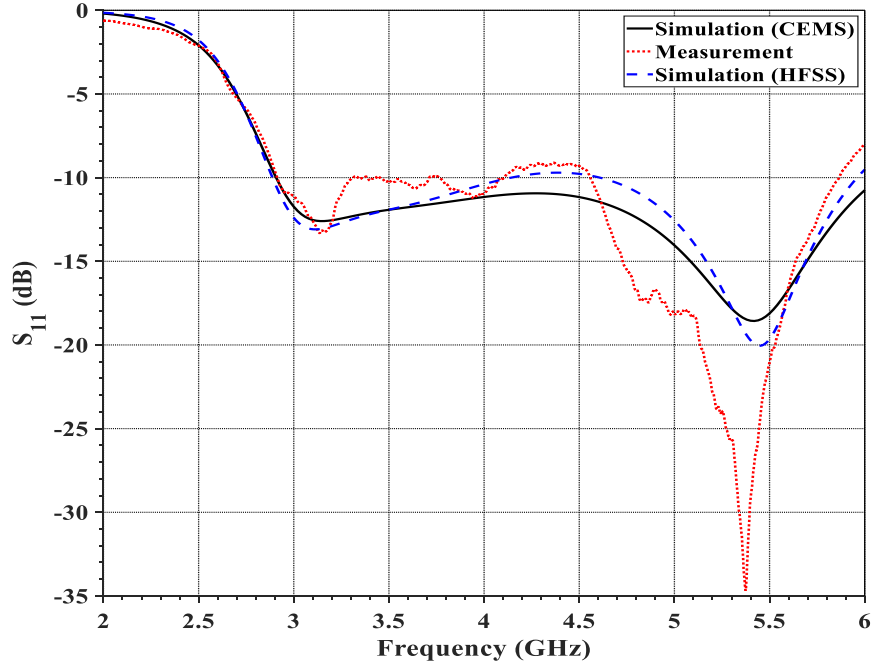


Figure 3.10: Simulated and measured S_{11} at the low frequency band.

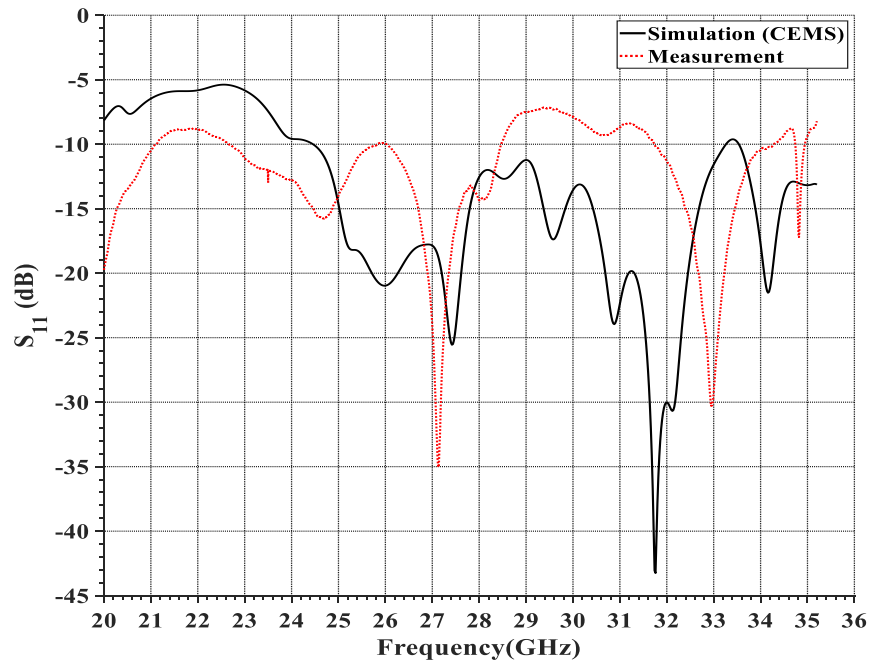


Figure 3.11: Simulated and measured S_{11} at the high frequency band.

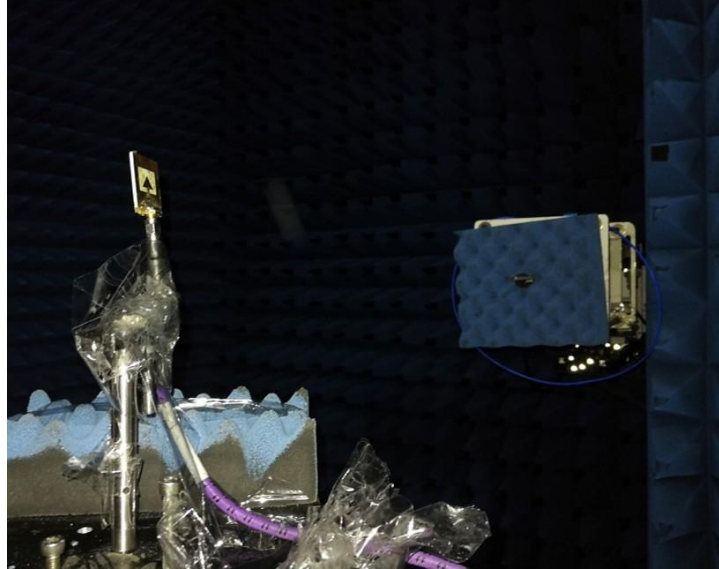


Figure 3.12: Antenna measurement in chamber.

For the high frequency band, the simulation is carried out through CEMS. Because HFSS uses the FEM algorithm, when the accuracy of the grid is large, the memory consumption is too high and accurate results were not possible to obtain with the current computer resources. Therefore, the FDTD algorithm with high accuracy and fast operation and low memory consumption is used. It is to be noticed that the SMA model is not established during the simulation. The measurement of S_{11} is conducted in the microwave chamber of Tsinghua University. The simulation and measurement results for the high frequency range vary because of different factors. Among these are the fact that the substrate material properties were not exactly known for the high frequency range, and the effects of the SMA size and the welding spots size relative to the antenna size. However, it is clearly visible that the main two resonances in this band are predicted by both the simulation and the measured results.

Simulations for the radiation pattern of the antenna were performed using CEMS and is shown in Figure 3.13. The 3D radiation pattern of the antenna at 3.7 GHz shows maximum gain of 3.8 dBi at the broadside ($\theta = 0^\circ$). Radiation pattern stability is also examined at two other frequencies, namely at 3.3 GHz and 3.9 GHz. These patterns in Figs. 3.14 and 3.15 show omnidirectional radiation in the H-plane and a dipole like radiation in the E plane. For the high-

frequency band, the radiation patterns at 28 GHz and 33 GHz are shown in Figs. 3.16 and 3.17 although no specific characteristics can be identified.

It is concluded through simulation and measurement that the feed structure, and arrow-patch have a greater influence on the S_{11} of the antenna, while the side structure has less influence on the S_{11} of the antenna.

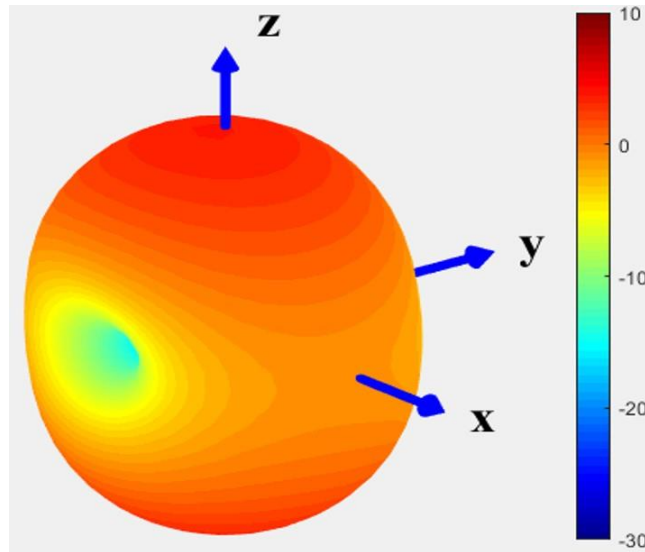


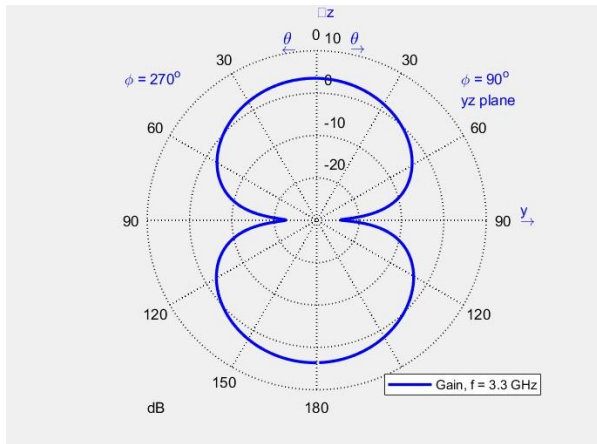
Figure 3.13: Simulated far-field radiation pattern at 3.7 GHz.

3.3 Chapter Summary

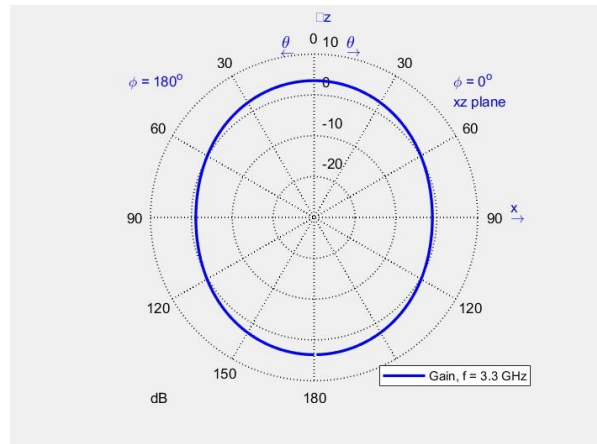
This chapter first proposes a wideband patch-slot antenna that uses a coplanar waveguide feed. Through the analysis and improvement of current distribution, simulation of different shapes of patches was optimized. Finally, the arrow-shaped antenna structure was decided on. The multi-frequency coplanar waveguide antenna designed in this chapter has good far-field radiation characteristics. Measurements show that the antenna can achieve the expected wide band input impedance results from the simulation at low frequency band. For the high-frequency band, there are some differences. However, the overall trends is the same considering the error that could be present due to the use of a substrate not supporting this high frequency, the exclusion of the SMA from the simulation, and the accuracy and setup of the measurement

in the high frequency chamber that we did not have control over. The measurements for the high frequency band were performed at Sichuan University and Tsinghua University, while the measurements for the lower frequency band use the facility of Colorado School of Mines.

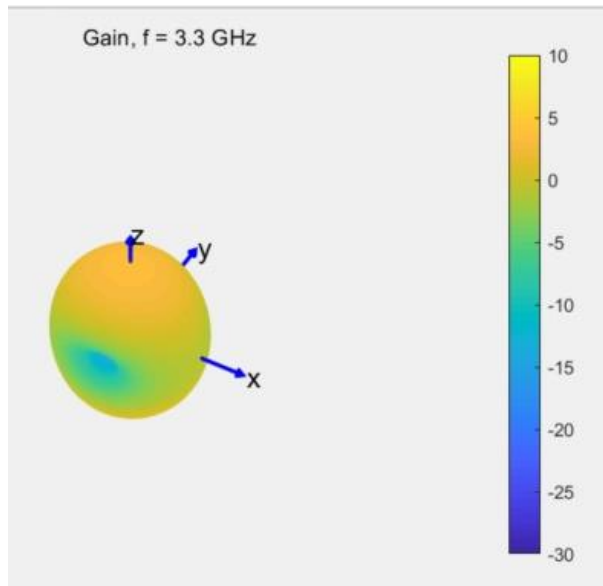
The antenna proposed in this chapter has a smaller size, and has obvious advantages compared with other antennas proposed in [36] and [37] for this same lower 5G band. Furthermore, the antenna has good potential to operate at both 5G low-frequency and high-frequency working bands, which solves the problem of using multiple different antennas for different working frequency bands. The antenna has relatively constant radiation characteristics at low frequencies.



(a) yz -plane (E -plane)

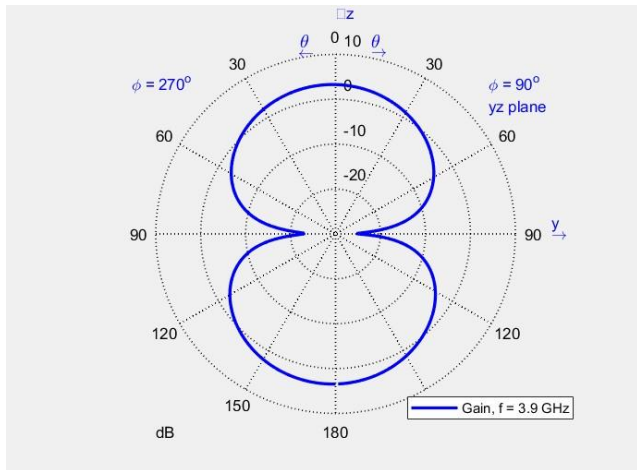


(b) Simulation xz -plane (H -plane)

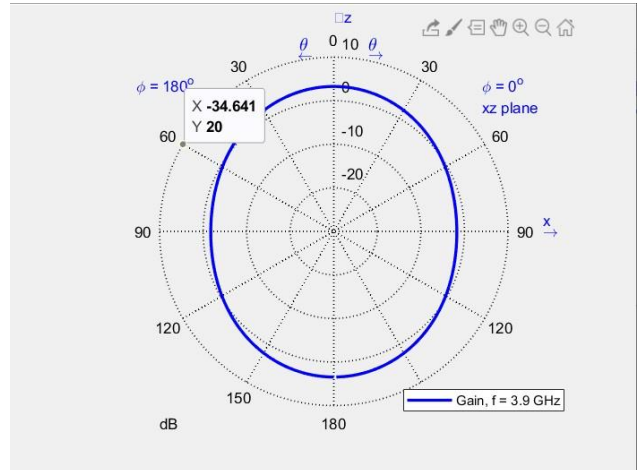


(c) Simulation 3D radiation pattern

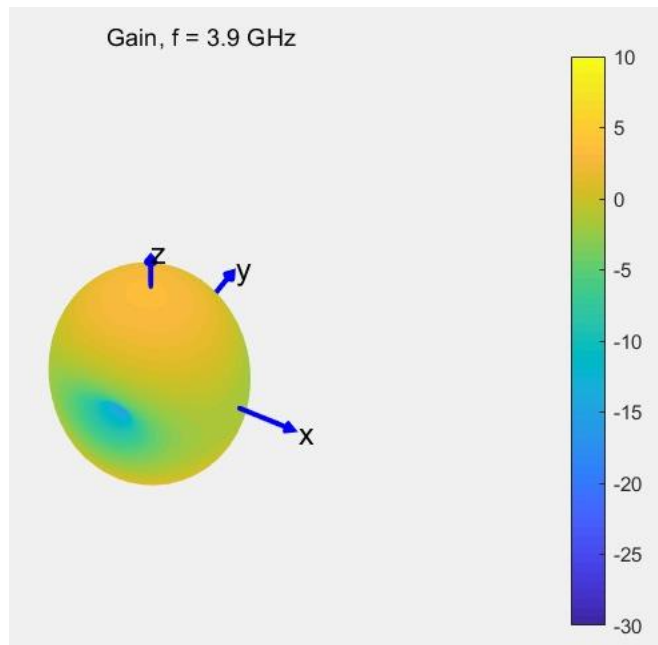
Figure 3.14: Simulated radiation pattern at 3.3 GHz.



(a) Simulation yz -plane (E -plane)

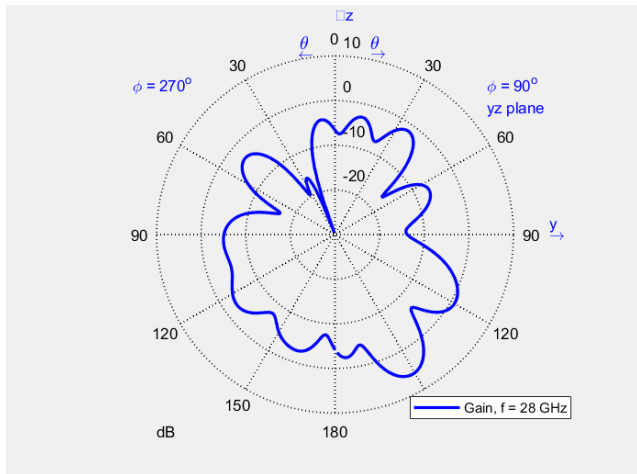


(b) Simulation xz -plane (H -plane)

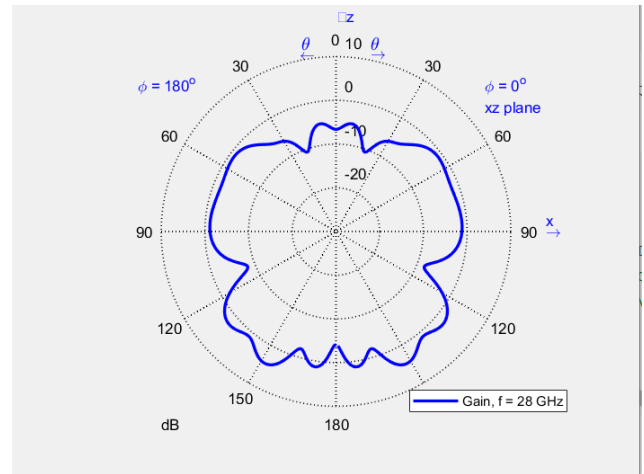


(c) Simulation 3D radiation pattern

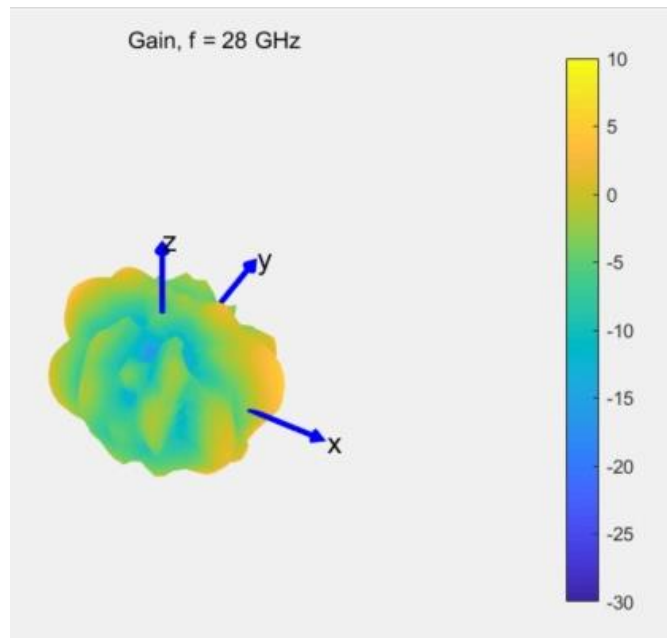
Figure 3.15: Simulated radiation pattern at 3.9 GHz



(a) Simulation yz -plane (E -plane)

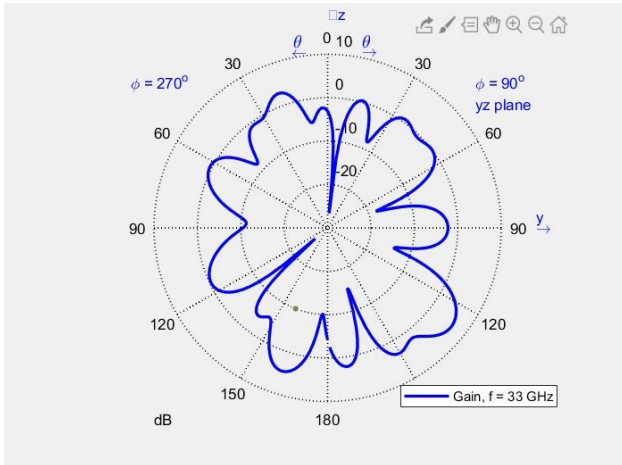


(b) Simulation xz -plane (H -plane)

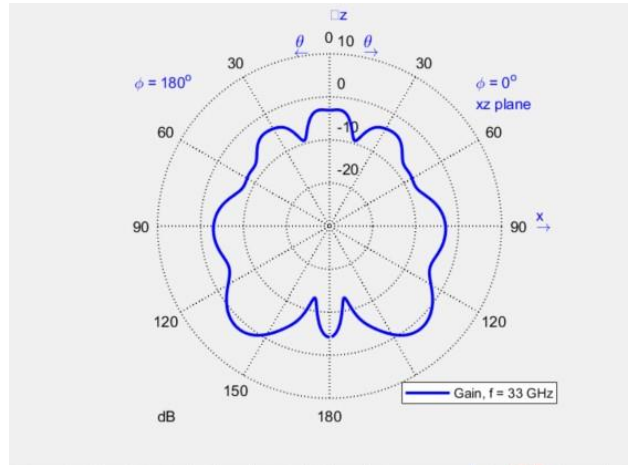


(c) Simulation 3D radiation pattern

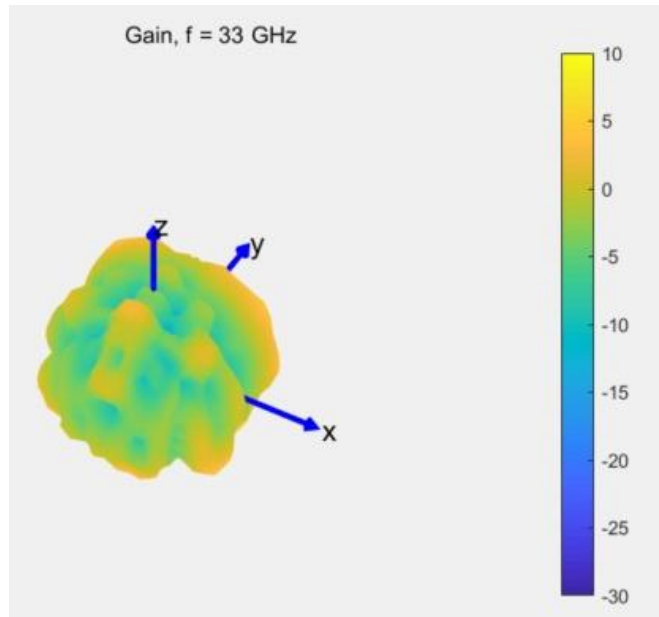
Figure 3.16: Simulated radiation pattern at 28 GHz.



(a) Simulation yz -plane (E -plane)



(b) Simulation xz -plane (H -plane)



(c) Simulation 3D radiation pattern

Figure 3.17: Simulated radiation pattern at 33 GHz.

CHAPTER 4

DESIGN OF ANTENNA ARRAY

4.1 Introduction

In recent years, due to the development of millimeter-wave and broadband technology, its own advantages such as high transmission rate and low power spectral density have made its application widely concerned, and significant development has been observed in less than ten years. A large amount of research work mainly focuses on how to achieve the miniaturization, wideband, and stable far-field characteristics. Because the communication system often encounters the phenomenon of multipath fading in the communication process, the receiving end will therefore receive multiple sets of signals with different delays, which will lead to the decrease of the overall gain of the system and the transmission rate. This is mainly because the electromagnetic waves propagate through different paths, the time for each component field to arrive at the receiving end is different, and the phases are superimposed on each other to cause interference, so that the original signal is distorted or an error occurs. Thus, using multiple-input multiple-output (MIMO) technology can effectively increase system gain. MIMO technology was first proposed by Marconi in 1908 [38]. It uses a structure of multiple antennas at the transmitting end and at the receiving terminal. Using this arrangement can greatly suppress the fading of the channel in the communication process, thereby improving the system channel capacity and increasing the coverage of the signal and the transmission rate of the channel. In the 1970s, it was proposed that this system can be used in communication networks. MIMO technology is a huge breakthrough in the field of wireless communications. In 2011, many companies developed WIFI or WIMAX commercial systems based on MIMO technology. In 2012, all 4G communication system standards (such as TD.LTE, LET.A, WIMAX, etc.) have selected MIMO [39–41] technology as one of its key technologies. The MIMO antenna uses multiple antennas at both the transmitting end and the receiving end. The transmission information stream passes through "space-time coding" to form Xn information sub-streams. The Xn sub-streams are sent to the channel at the same time, and each transmitted signal

occupies the same frequency band, so the system bandwidth is not increased. If the channel response of each transmitting and receiving antenna is independent, the multiple-input multiple-output system can create multiple parallel spatial channels. By transmitting information independently through these parallel spatial channels, the data rate will inevitably be increased. Thus, the study of an array of antenna can be considered as a larger scale of few multiple antennas in a MIMO system. This array can be at either the transmitting or the receiving end. Compared to what can be achieved with a single element, an antenna array can achieve higher gain (directivity), that is, a narrower radio beam. Generally, the larger the number of individual antenna elements used, the higher the gain and the narrower the radiated beam.

In this chapter, in order to improve the directivity and practicability of the designed antenna, an antenna array is investigated. The array is designed based on the antenna element designed in the previous chapter. An antenna array working in the 5G low frequency band is designed using computer simulations. The array has a compact structure and stable radiation characteristics in the working frequency range, which meets the requirements of 5G communications.

4.2 Design of Antenna Array Based on Arrow Patch-slot Antenna Element

The unit structure of the antenna is the structure designed in the previous chapter. First, a 5-elements linear antenna array along the x-axis is designed as shown in Figure 4.1. The antenna elements are separated by one-half of a wavelength or less at 3.7 GHz. When the array element spacing is greater than half a wavelength, grating lobes appear and therefore, our design is limiting the separation between the centers of the elements to less than half wavelength. In order to demonstrate the potential of this element in building phased array base station antennas with miniaturization and broadband capabilities, the linear array was also simulated using 15-elements as shown in Figure 4.2. The simulation is performed using the two independent software packages HFSS and CEMS for verification of the simulation results and because of the suitability (computer resources and simulation time required by each) of each package to the configuration to be studied.

4.2.1 Theoretical basis of antenna array

As shown in Fig. 4-1, assume that the array element spacing of the linear array along the x axis is d , the number of array elements is N , and the beam pointing angle is θ . The wave path difference is then $d\sin\theta, 2d\sin\theta, \dots, nd\sin\theta$. The array factor according to the superposition principle is:

$$AF_{linear}(\theta, \varphi) = \sum_{n=1}^N \alpha_n \cdot e^{j(\beta_n + k \cdot d \cdot n \cdot \sin \theta)} \quad (4.1)$$

$$\Delta\beta(\theta_0) = -kd \cdot \sin \theta_0 \quad (4.2)$$

$$\beta(\theta_0) = -kd \cdot n \cdot \sin \theta_0 \quad (4.3)$$

$$|AF_{linear}(\theta, \theta_0)| = \left| \frac{\sin\left(\frac{N}{2} \cdot k \cdot d \cdot (\sin \theta - \sin \theta_0)\right)}{\sin\left(\frac{k \cdot d \cdot (\sin \theta - \sin \theta_0)}{2}\right)} \right| \quad (4.4)$$

where k is the wave number, θ_0 is the desired scanned angle in the x - z plane.

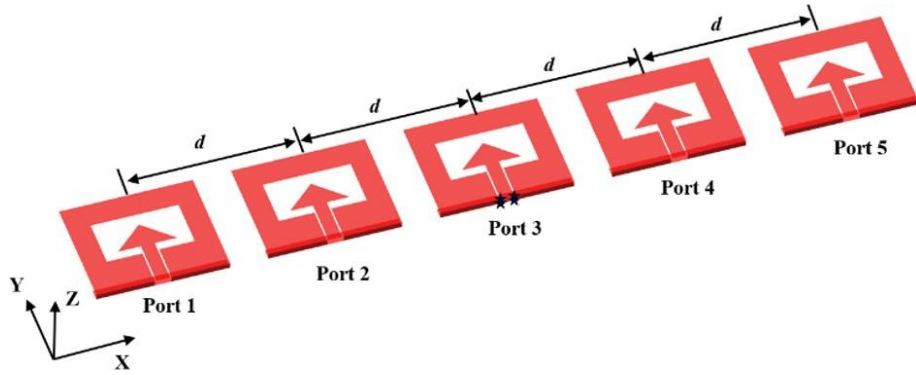


Figure 4.1: Configuration of a linear of 5-elements using CEMS.

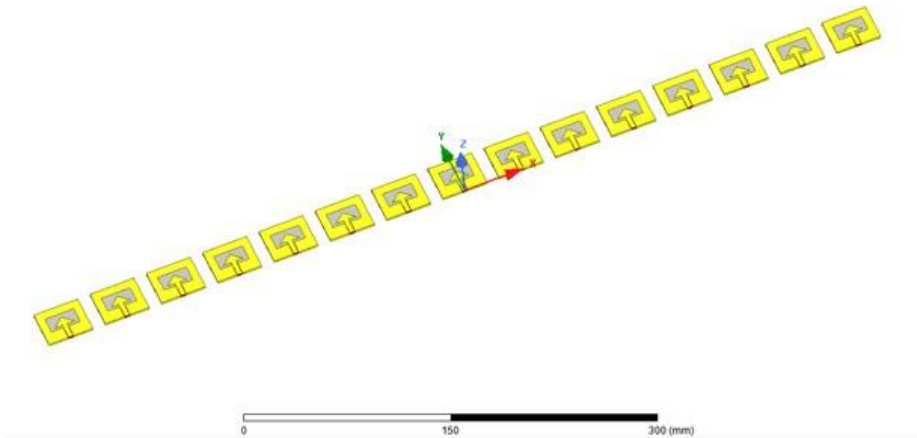


Figure 4.2: Configuration of a linear array of 15-elements using HFSS.

4.2.2 Basic structure configuration and parameter analysis of antenna array

Base stations antennas of many of our cellular wireless systems [42, 43] and PCS [44, 45] systems consist of line arrays. In communication systems, especially in a point-to-point communication system, the antenna is required to have relatively strong directivity, that is, the antenna can concentrate most of the energy to radiate in a predetermined direction. As the length of the array increases, the main lobe of its pattern becomes narrower. The directivity will be better, but when the electrical length between the centers of the elements is greater than half wavelength of the operating frequency, grating lobes appear, and becomes larger than the main lobe. In the antenna array, the radiation direction, gain, isolation and return loss are important indicators. In the design of this antenna array, first we consider the return loss, because the working frequency suitable for 5G is our goal, and then we need to ensure that the coupling between elements is in the order of at least -20 dB at the desired operating frequency by first adjusting the spacing between the array elements to have good isolation. However, the spacing also affects the antenna gain. Hence the antenna array is simulated and optimized numerically to have better gain and scanning range without grating lobes.

4.2.3 Analysis of simulation results of antenna array

When the antenna is simulated using CEMS the reflection coefficient of the linear array at port 3, the center element in the 1×5 array, is shown in Figure 4.3. Due to the symmetrical property of the linear array displacement along x direction, the S-parameter results of port 4 and 5 have the same performance as the results of port 2 and 1, respectively.

The results in Fig. 4.3 show that the designed 5-elements linear array supports the operation in the sub-6GHz bands while maintaining coupling among the elements in the order or less than -20 dB.

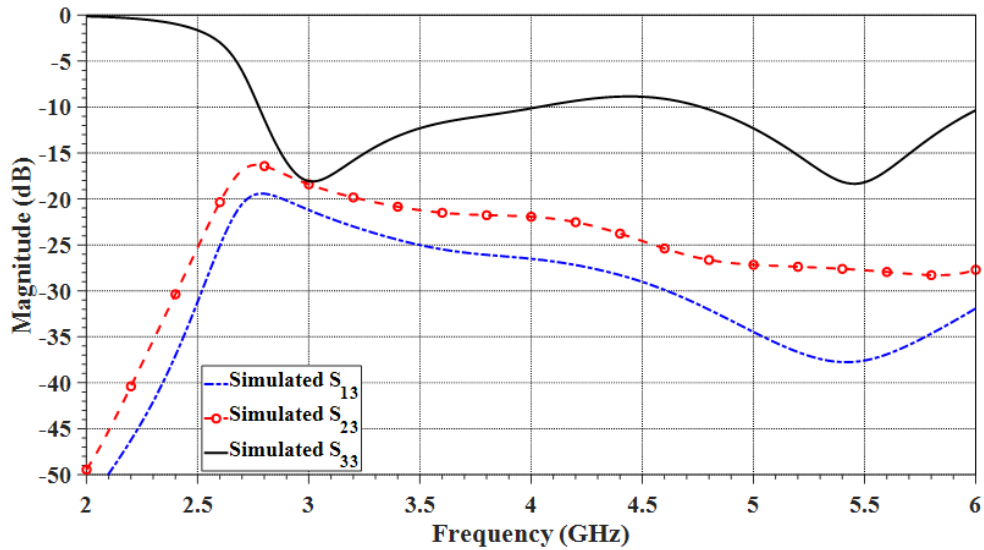


Figure 4.3: S parameter at roots for the 1×5 linear arrays.

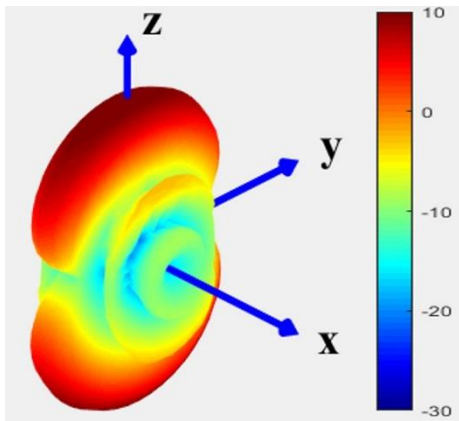
Through antenna array equations (4.1) - (4.3), we get the excitation phase for the required main beam scanned direction. Figs. 4.4 to 4.6 show the radiation of the antenna for different excitations defined in Tables 4.1 and 4.2. The excitation phase (degree) and relative excitation phase (degree) are calculated for 0° , 30° , 45° scanned beam. It is obvious that 5 elements are not sufficient to produce a scanned beam beyond 30° degrees without having large side lobes that are comparable to the main lobe level.

Table 4.1: Excitation setting for (30° scanned beam)

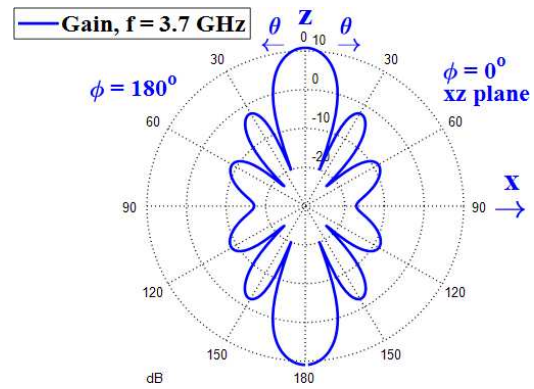
Element number	Excitation Amplitude (degree)	Excitation Phase (degree)	Relative Excitation Phase (degree)
n=1	1	260.1	200
n=2	1	160.2	100
n=3	1	60.3	0
n=4	1	320.4	260
n=5	1	220.5	160

Table 4.2: Excitation setting for (45° scanned beam)

Element number	Excitation Amplitude (degree)	Excitation Phase (degree)	Relative Excitation Phase (degree)
n=1	1	218.72	282
n=2	1	77.44	141
n=3	1	296.16	0
n=4	1	154.88	228
n=5	1	13.60	77

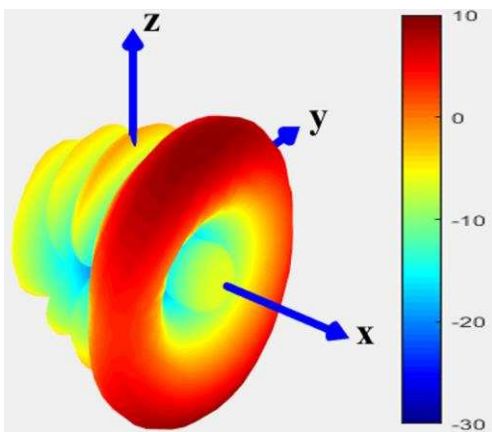


(a) Gain Pattern 3D

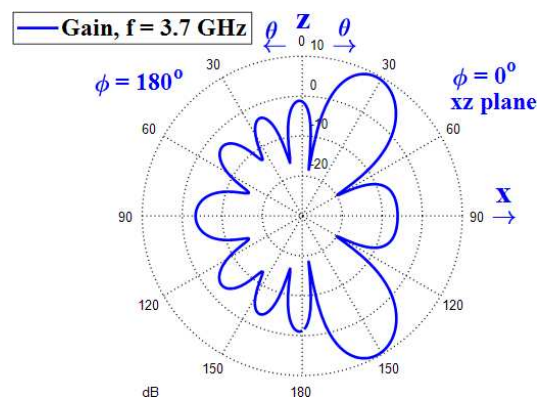


(b) Gain Pattern xz

Figure 4.4: 5 elements liner array gain pattern at 3.7 GHz, uniform excitation with 0° main beam directions



(a) Gain Pattern 3D



(b) Gain Pattern xz

Figure 4.5: 5 elements liner array gain pattern at 3.7 GHz with uniform excitation and 30° main beam directions.

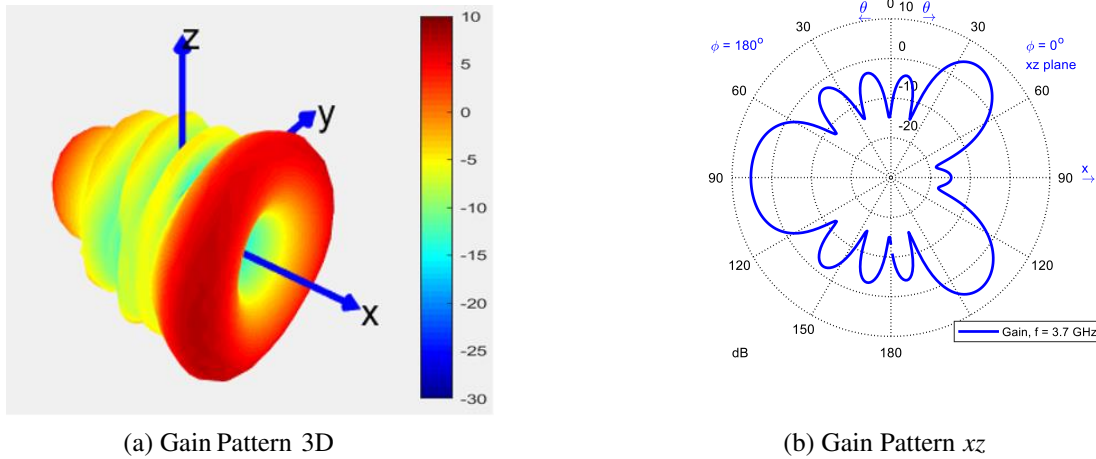


Figure 4.6: 5 elements linear array gain pattern at 3.7 GHz with uniform excitation and 45° main beam directions.

As the number of components in a linear array configuration increases, higher gains and larger scanning ranges can be obtained without significant reductions in S-parameters or far field characteristics. Good element-to-element isolation was observed, and the scanning ability of more elements could be predicted. To pursue better directivity and gain, the number of antenna elements is increased to 15 elements with a total array size smaller than 8.31λ (66.5cm) at 3.7 GHz. The simulated S parameters of the 1×15 linear arrays at the center port (port 8) are shown in Fig. 4.7. From this figure, the antenna input reflection at port 8 is less than -10 dB, and the strongest coupling between ports 8 and 7 is in the order of -19 dB, at operating frequency of 3.7 GHz.

The relationship between the excitation phase at each element for the 45° and 60° scanned beams is listed in Table 4.3 and 4.4. The simulated gain pattern of 1×15 linear arrays is shown in Figs 4.8 to 4.10 at 3.7GHz for 0° , 45° , 60° scanned beam. It is obvious here that the 45° is yielding a better pattern than the one with the 5 elements, while the 60° case requires more elements to avoid the resulting large side lobe level.

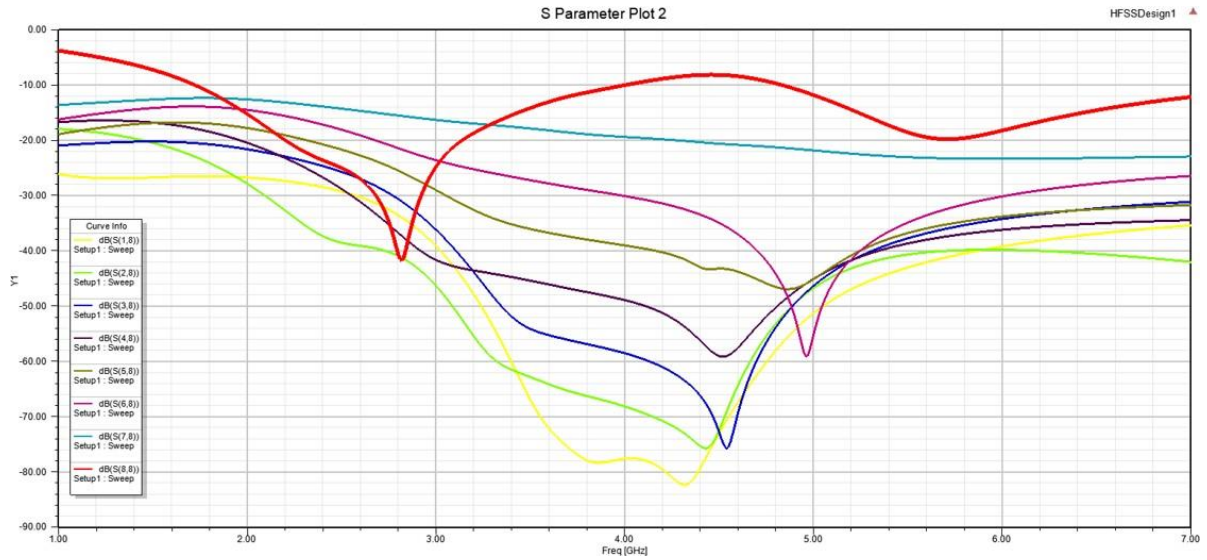


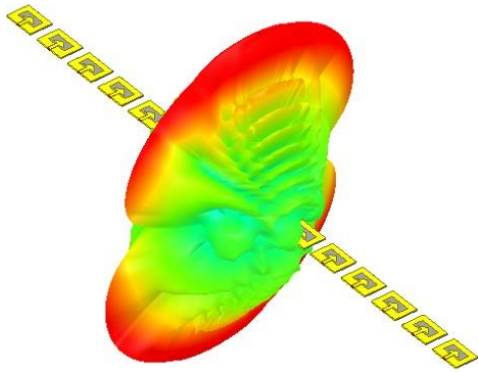
Figure 4.7: S parameters at port 8 of a 15-element linear array using HFSS.

Table 4.3: Excitation setting for 45° scanned beam

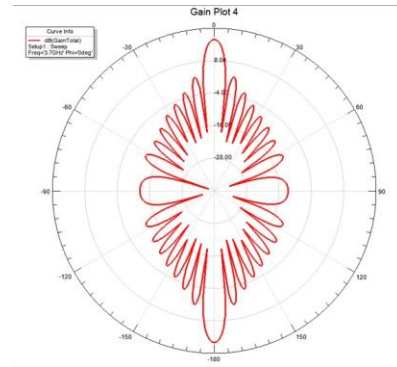
Element number	Excitation Amplitude (degree)	Excitation Phase (degree)	Relative Excitation Phase (degree)
n=1	1	218.72	268.96
n=2	1	77.44	127.68
n=3	1	296.16	346.4
n=4	1	154.88	205.12
n=5	1	13.60	63.84
n=6	1	232.32	282.56
n=7	1	91.04	141.28
n=8	1	309.76	0
n=9	1	168.48	218.72
n=10	1	27.20	77.44
n=11	1	245.92	296.16
n=12	1	104.64	154.88
n=13	1	323.36	13.6
n=14	1	182.08	232.32
n=15	1	40.80	91.04

Table 4.4: Excitation setting for 60° scanned beam

Element number	Excitation Amplitude (degree)	Excitation Phase (degree)	Relative Excitation Phase (degree)
n=1	1	186.97	131.22
n=2	1	13.94	318.19
n=3	1	200.90	145.15
n=4	1	27.87	332.12
n=5	1	214.84	159.09
n=6	1	41.81	346.06
n=7	1	228.78	273.03
n=8	1	55.75	0
n=9	1	242.71	186.96
n=10	1	69.68	13.93
n=11	1	256.65	200.9
n=12	1	83.62	27.87
n=13	1	270.59	214.84
n=14	1	97.55	41.80
n=15	1	284.52	228.77

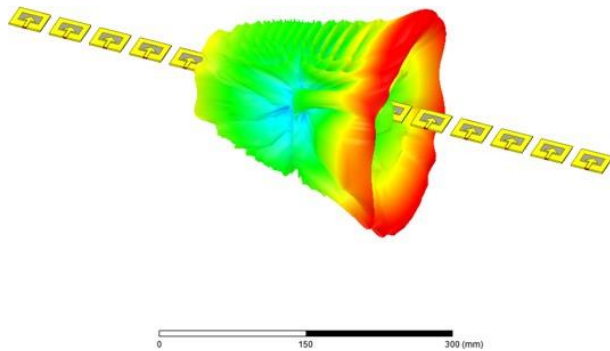


(a) 3D gain pattern

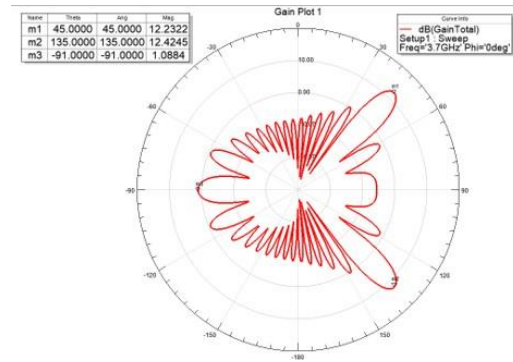


(b) Gain pattern in xz -plane

Figure 4.8: 15 elements liner array Gain Pattern at 3.7 GHz, uniform excitation with 0° main beam directions

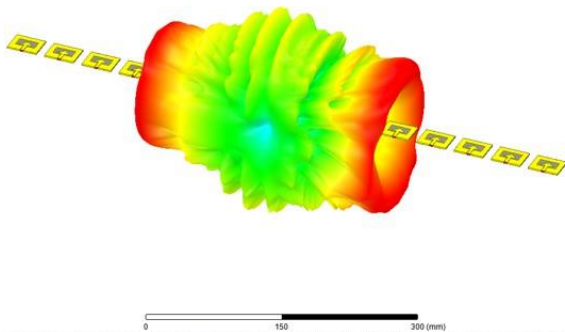


(a) 3D gain pattern

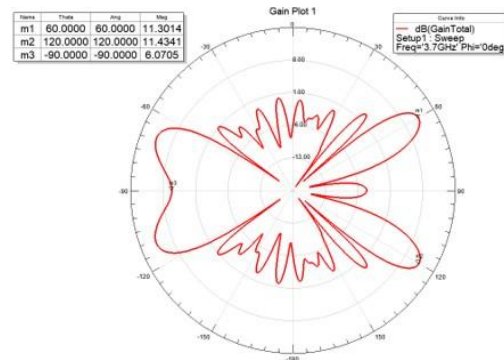


(b) Gain pattern in xz -plane

Figure 4.9: 15 elements liner array gain pattern at 3.7 GHz with uniform excitation and 45° main beam directions.



(a) 3D gain pattern



(b) Gain pattern in xz -plane

Figure 4.10: 15 elements liner array gain pattern at 3.7 GHz with uniform excitation and 60° main beam directions.

Finally, the gains of different excitation setting and number of elements in the array can be seen in Table 4.3. In general, the increase in gain mainly depends on reducing the width of the main radiating lobe in the x - z plane while maintaining the omnidirectional radiation performance on the y - z plane. Increasing the gain can increase the range coverage of the network in a certain direction. The antenna gain of the GSM directional base station is usually in the order of 18dBi.

Table 4.5: Broadside gain at 3.7 GHz

Element numbers (N)	Main Beam Direction (degree)	Gain (dBi)
N=1	0	3.8
N=5	0	10.9
N=5	30	9.4
N=15	0	16
N=15	45	12.4

4.3 Chapter Summary

In this chapter, 5-elements and 15 elements linear arrays are designed based on the previous unit antenna element to increase the gain for operation in the low band of the 5G at 3.7 GHz. The coupling, gain, and scanning features are simulated and presented, showing good performance for base station antenna applications.

CHAPTER 5

CONCLUSIONS AND OUTLOOK

5.1 Summary

Based on the design principle of a microstrip patch antenna, a multi-band antenna based on a patch-slot combination for 5G equipment is proposed. This thesis introduces an arrow patch-slot antenna design operating at the 5G low and high frequency bands at the same time. The design is based on coplanar waveguide feeding structure. This research mainly revolves around the antenna's structure and its function characteristics. Because the performance of the antenna obtained by simulation is good and the structure is not complicated, a prototype of the antenna is manufactured and measured. Measurements were conducted whenever the facilities are available and good comparison is obtained, especially in the low frequency band of the 5G operating frequencies. From the final measurement results, the bandwidth of the antenna is 2.9 – 5.9 GHz, which fully includes the low-frequency licensed for 5G in the US. In the meantime, the antenna's high-frequency 24 – 40GHz also includes the 5G high-frequency standard, so the antenna can simultaneously act on multiple 5G frequency bands. The antenna radiation performance can also be seen from the simulation results. At low frequencies, the antenna has good and stable gain, good directivity and omnidirectional characteristics in two orthogonal planes.

In order to meet the antenna directivity requirements of base stations, antenna array configurations were considered. Based on the single antenna element design. Two linear arrays were designed, and the simulation results were obtained. Good element-to-element isolation was observed, and the scanning capabilities of the linear array was demonstrated through numerical simulations.

5.2 Future Work

Further research can focus on the directionality of the antenna element. For this a suggested cavity backed configuration is proposed as shown in Fig. 5.1. The bottom of the cavity is a rectangle with dimensions of 11.51 mm by 10.88 mm. The resulting S_{11} curve using HFSS and CST is shown in Figure 5.2. Good match is observed for the 5G low band operation.

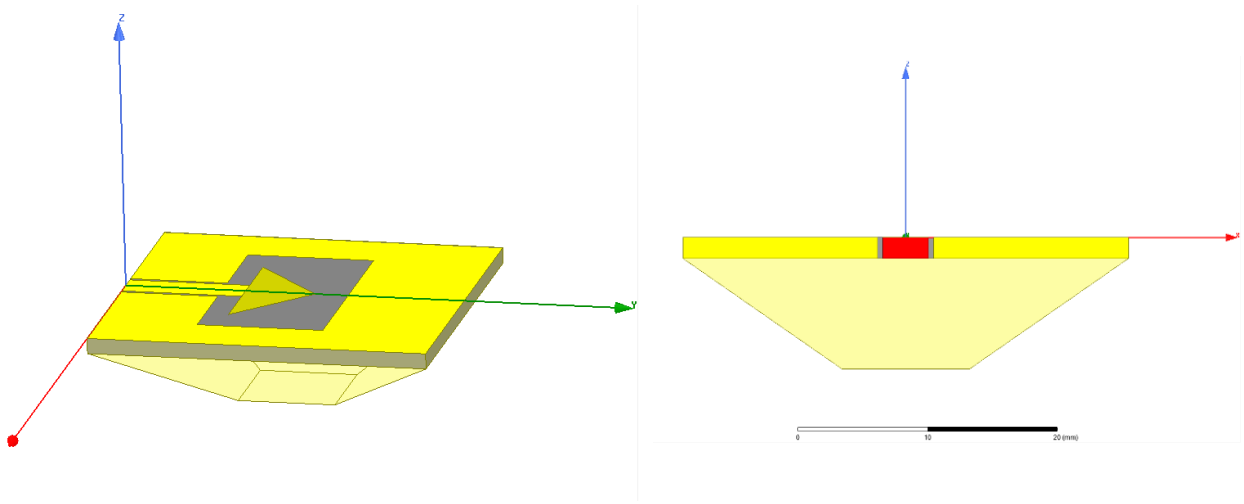


Figure 5.1: Cavity backed arrowhead slot antenna for unidirectional radiation pattern.

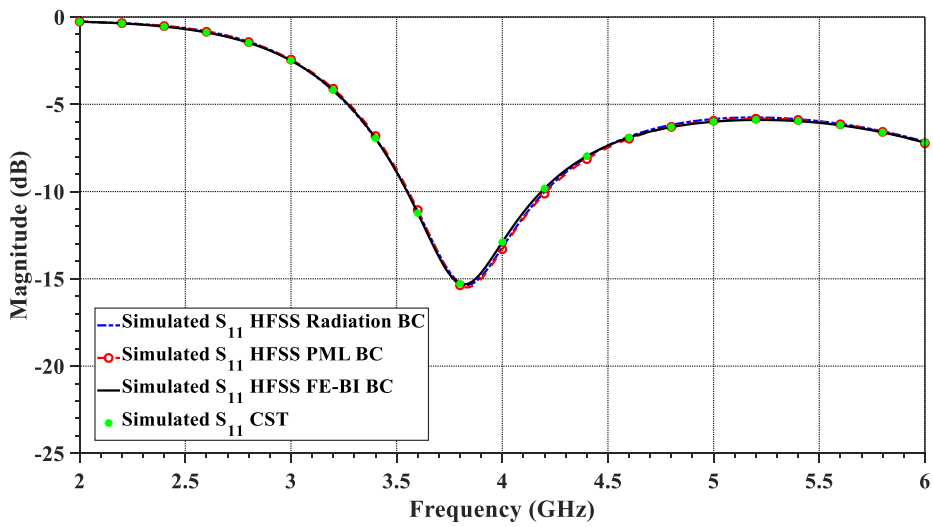


Figure 5.2: S_{11} of cavity backed arrowhead slot antenna.

Additionally, the extension of the linear array to two-dimensional array would be useful to study the possibility of implementing two-dimensional electronically beam scanning feature.

REFERENCES CITED

- [1] FCC, “5G Americas Spectrum Recommendations for the U.S.”, <https://www.5Gamericas.org/5G-americas-spectrum-recommendations-for-the-u-s/>, July 2019.
- [2] F. Farzami, K. Forooraghi, and M. Norooziarab, “Miniaturization of a Microstrip Antenna Using a Compact and Thin Magneto-Dielectric Substrate”. *IEEE Antennas and Wireless Propagation Letters*, 10: pp. 1540–1542, 2011.
- [3] H. Mosallaei and K. Saraband, “Antenna miniaturization and bandwidth enhancement using a reactive impedance substrate,” *IEEE Transactions on Antennas and Propagation*, 52(9): pp. 2403–2414, Sep. 2004.
- [4] A. Bakhmutov, N. Knyazev, and V. Chechetkin, “Reconfigurable electrically small split ring resonator antenna,” pp. 1–2, March 2017.
- [5] A. Romputtal and C. Phongcharoenpanich, “Frequency reconfigurable multiband antenna with embedded biasing network,” *IET Microwaves, Antennas Propagation*, 11 (10): pp.1369–1378, 2017.
- [6] P. Fernandez-Martinez, S. Martin-Anton, and D. Segovia-Vargas, “Design of a Wide-band Vivaldi Antenna for 5G Base Stations,” pp. 149–150, July 2019.
- [7] S. X. Ta, H. Choo, and I. Park, “Broadband Printed-Dipole Antenna and Its Arrays for 5G Applications,” *IEEE Antennas and Wireless Propagation Letters*, 16: pp. 2183–2186, 2017.
- [8] Zhinong Ying, “Antennas in Cellular Phones for Mobile Communications,” *Proceedings of the IEEE*, 100: pp. 2286–2296, 2012.
- [9] N. Luo, Y. He, L. Zhang, S. Wong, C. Li and Y. Huang, "A Differential Broadband Dual-Polarized Base Station Antenna Element for 4G And 5G Applications," *2019 Computing, Communications and IoT Applications (ComComAp)*, pp. 337-340, 2019.
- [10] K. C. Gupta, Jun Li, R. Ramadoss, and Chunjun Wang, “Design of frequency- reconfigurable rectangular slot ring antennas,” 1: pp. 326 vol. 1, July 2000.
- [11] J. Zeng and K. Luk, "Single-Layered Broadband Magnetolectric Dipole Antenna for New 5G Application," in *IEEE Antennas and Wireless Propagation Letters*, vol. 18, no. 5, pp. 911-915, May 2019.
- [12] J. L. Freeman, B. J. Lamberty, and G. S. Andrews. “Optoelectronically reconfigurable monopole antenna,” *Electronics Letters*, 28(16): pp. 1502–1503, July 1992.
- [13] Z. Nie, H. Zhai, L. Liu, J. Li, D. Hu, and J. Shi, “A Dual-Polarized Frequency- Reconfigurable Low-Profile Antenna With Harmonic Suppression for 5G Application”. *IEEE Antennas and*

Wireless Propagation Letters, 18(6): pp. 1228–1232, June 2019.

- [14] S. Hur, S. Baek, B. Kim, Y. Chang, A. F. Molisch, T. S. Rappaport, K. Haneda, and J. Park, “Proposal on Millimeter-Wave Channel Modeling for 5G Cellular System,” *IEEE Journal of Selected Topics in Signal Processing*, 10(3): pp. 454–469, April 2016.
- [15] Jin-Sen Chen, “Studies of CPW-fed equilateral triangular-ring slot antennas and triangular-ring slot coupled patch antennas,” *IEEE Transactions on Antennas and Propagation*, 53(7):pp. 2208–2211, July 2005.
- [16] T. Reck, R. M. Weikle, and N. S. Barker. “A Waveguide to Unenclosed Coplanar Waveguide Transition,” *IEEE Transactions on Microwave Theory and Techniques*, 58 (9): pp. 2420–2425, Sep. 2010.
- [17] V. S. Mottonen. “Wideband coplanar waveguide-to-rectangular waveguide transition using fin-line taper”. *IEEE Microwave and Wireless Components Letters*, 15(2): pp. 119–121, Feb 2005.
- [18] Y. Ding, Y. C. Jiao, P. Fei, B. Li, and Q. T. Zhang, “Design of a Multiband Quasi- Yagi-Type Antenna With CPW-to-CPS Transition,” *IEEE Antennas and Wireless Propagation Letters*, 10: pp. 1120–1123, 2011.
- [19] G. Li, H. Zhai, T. Li, L. Li, and C. Liang, “CPW-Fed S-Shaped Slot Antenna for Broadband Polarization,” *IEEE Antennas and Wireless Propagation Letters*, 12: pp. 619–622, 2013.
- [20] Eldek. Abdelnasser, Elsherbeni. Atef, and Smith, Charles, “Two-dimensional array of rectangular slot antennas tuned with patch stubs for wide bandwidth and large scanning range,” *Microwave and Optical Technology Letters*, 45: pp. 149 - 152, 2005.
- [21] Eldek. Abdelnasser, Elsherbeni. Atef, and Smith, Charles, “Wideband 2D array of microstrip fed rectangular slot antenna for radar applications,” *Microwave and Optical Technology Letters*, 46: pp. 36 - 40, 2005.
- [22] A. A. Eldek, A. Z. Elsherbeni, C. E. Smith and Kai-Fong Lee, "Wideband rectangular slot antenna for personal wireless communication systems," in *IEEE Antennas and Propagation Magazine*, 44(5): pp. 146-155, Oct. 2002.
- [23] C. P. Wen, “Coplanar Waveguide, a Surface Strip Transmission Line Suitable for Non-reciprocal Gyromagnetic Device Applications,” pp. 110–115, May 1969.
- [24] Y. Lin and K. Hung, “Compact Ultra-wideband Rectangular Aperture Antenna and Band-Notched Designs,” *IEEE Transactions on Antennas and Propagation*, 54(11): pp. 3075–3081, Nov 2006.
- [25] G. Gao, B. Hu, and J. Zhang, “Design of a Miniaturization Printed Circular-Slot UWB Antenna by the Half-Cutting Method,” *IEEE Antennas and Wireless Propagation Letters*, 12: pp.

567–570, 2013.

- [26] Wikipedia. “Biconical antenna”. https://en.wikipedia.org/wiki/Biconical_antenna, Dec 2019.
- [27] “Novel Modified Pythagorean Tree Fractal Monopole Antennas for UWB Applications,” *IEEE Antennas and Wireless Propagation Letters*, 10: pp. 484–487, 2011.
- [28] Hojjat Fallahi and Zahra Atlasbaf, “Study of a Class of UWB CPW-Fed monopole antenna with fractal elements,” *Antennas and Wireless Propagation Letters, IEEE*, 12: pp. 1484–1487, 01 2013.
- [29] Abhik Gorai, Manimala Pal, and Rowdra Ghatak, “A Compact Fractal-Shaped Antenna for Ultrawideband and Bluetooth Wireless Systems with WLAN Rejection Functionality,” *IEEE Antennas and Wireless Propagation Letters*, 16: pp. 2163–2166, 2017.
- [30] Charlotte Marchais, G. Le Ray, L. Lecoq, and Ala Sharaiha, “A Stripline Fed Printed Wide Slot Antenna for UWB Applications,” *2006 12th International Symposium on Antenna Technology and Applied Electromagnetics and Canadian Radio Sciences Conference*, pp. 1–4, 2006.
- [31] Seong Jae Jeong and Keum Cheol Hwang, “Circular hook-shaped wireless USB dongle antenna with an open stub,” *IEICE Electronics Express*, 7(18): pp. 1370–1375, 2010.
- [32] Tzyh-Ghuang Ma and Shyh-Kang Jeng, “Planar miniature tapered-slot-fed annular slot antennas for ultrawide-band radios,” *IEEE Transactions on Antennas and Propagation*, 53: pp. 1194–1202, 2005.
- [33] Constantine A. Balanis, “*Antenna Theory Analysis and Design*,” *Fourth Edition*, John Wiley, United States of America, 2016.
- [34] V. Demir and A. Elsherbeni, CEMS Software package, Version 4, 2019.
- [35] Atef Elsherbeni and Veysel Demir, *The Finite Difference Time Domain Method for Electromagnetics with MATLAB Simulations*, ACES Series on Computational Electromagnetics and Engineering, SciTech Publishing Inc. an Imprint of the IET, Second Edition, Edison, NJ, 2015.
- [36] S. Martin-Anton and D. Segovia-Vargas, "Fully Planar Dual-Polarized Broadband Antenna for 3G, 4G and Sub 6-GHz 5G Base Stations," in *IEEE Access*, vol. 8, pp. 91940-91947, 2020.
- [37] C. Hsiao and W. Chen, "Broadband Dual-Polarized Base Station Antenna for LTE/5G C-band Applications," *2018 Cross Strait Quad-Regional Radio Science and Wireless Technology Conference (CSQRWC), Xuzhou*, pp. 1-3, 2018.
- [38] S. G. Marconi, “Radio Telegraphy,” *Proceedings of the Institute of Radio Engineers*, 10 (4): pp.

215–238, Aug 1922.

- [39] O. K. Sharma, Shankar T., and P. Krishnatre, “Reducing interference of Gaussian MIMO Z channel and Gaussian MIMO X Channel,” pp. 977–980, March 2016.
- [40] Y. Zhang, J. Deng, M. Li, D. Sun, and L. Guo, “A MIMO Dielectric Resonator Antenna with Improved Isolation for 5G mm-Wave Applications,” *IEEE Antennas and Wireless Propagation Letters*, 18(4): pp. 747–751, April 2019.
- [41] Z. Ren, A. Zhao, and S. Wu, “MIMO Antenna With Compact Decoupled Antenna Pairs for 5G Mobile Terminals,” *IEEE Antennas and Wireless Propagation Letters*, 18 (7): pp. 1367–1371, July 2019.
- [42] A. Alsohaily and E. S. Sousa, “The Omitted Dimension: Exploiting Multiuser Diversity in Multi-Radio Access Technology Data Cellular Communication Systems,” *IEEE Access*, 4:pp. 2068–2082, 2016.
- [43] W. Tuttlebee, “You’ll never talk alone [cellular radio networks],” *IEE Review*, 43(3): pp. 99–102, May 1997.
- [44] T. Chu and L. J. Greenstein, “A semi-empirical representation of antenna diversity gain at cellular and PCS base stations,” *IEEE Transactions on Communications*, 45 (6): pp. 644–646, June 1997.
- [45] J. Weitzen and M. Wallace, “Analysis of diversity performance of space diversity and cross polarization for PCS base stations,” 1: pp. 293–297 vol.1, Sep. 1998.